Received Dec. 9 2009; Accepted June 1 2010
Preprint typeset using LaTeX style emulateapj v. 11/10/09

THE IMPACT OF COLD GAS ACCRETION ABOVE A MASS FLOOR ON GALAXY SCALING RELATIONS

N. Bouché[1,2], A. Dekel[3], R. Genzel[1], S. Genel[1], G. Cresci[1,4], N. M. Förster Schreiber[1] , K. L. Shapiro[5] , R. I. Davies[1] , L. Tacconi[1]

Received Dec. 9 2009; Accepted June 1 2010

ABSTRACT

Using the cosmological baryonic accretion rate and normal star formation (SF) efficiencies, we present a very simple model for star-forming galaxies (SFGs) that accounts for the mass and redshift dependences of the SFR-Mass and Tully-Fisher (TF) relations from $z \sim 2$ to the present. The time evolution follows from the fact that each modeled galaxy approaches a steady state where the SFR follows the (net) cold gas accretion rate. The key feature of the model is a halo mass floor $M_{\rm min} \simeq 10^{11}\ M_\odot$ below which accretion is quenched in order to simultaneously account for the observed slopes of the SFR-Mass and TF relations. The same successes cannot be achieved via a star-formation threshold (or delay) nor by varying the SF efficiency or the feedback efficiency. Combined with the mass ceiling for cold accretion due to virial shock heating, the mass floor $M_{\rm min}$ explains galaxy "downsizing", where more massive galaxies formed earlier and over a shorter period of time. It turns out that the model also accounts for the observed galactic baryon and gas fractions as a function of mass and time, and the cosmic SFR density, which are all resulting from the mass floor $M_{\rm min}$. The model helps to understand that it is the cosmological decline of accretion rate that drives the decrease of cosmic SFR density between $z \sim 2$ and $z = 0$ and the rise of the cosmic SFR density from $z \sim 6$ to $z \sim 2$ allows us to put a constraint on our main parameter $M_{\rm min} \simeq 10^{11}\ M_\odot$. Among the physical mechanisms that could be responsible for the mass floor, we view that photo-ionization feedback (from first in-situ hot stars) lowering the cooling efficiency is likely to play a large role.

Subject headings: cosmology: observations — galaxies: high-redshift — galaxies: evolution

1. INTRODUCTION

To a good first order approximation, galaxies are either blue and active or red and passive, as indicated by the color bi-modality. In the past few years, it has been realized that blue star-forming galaxies (SFGs) lie on a tight relationship between their stellar mass $M_\star$ and star-formation rate (SFR) (Bell et al. 2005; Elbaz et al. 2007; Noeske et al. 2007a; Daddi et al. 2007; Drory & Alvarez 2008; Chen et al. 2009; Santini et al. 2009; Pannella et al. 2009; Damen et al. 2009b; Oliver et al. 2010). This SFR-$M_\star$ relationship is analogous to the red sequence for passively evolving galaxies and is sometimes referred to as the *SFR sequence*. Every multi-wavelength survey has shown that the specific SFR (sSFR≡SFR/$M_\star$) is higher for lower mass SFGs (e.g. Brinchmann et al. 2004; Bell et al. 2005; Noeske et al. 2007a; Drory & Alvarez 2008; Oliver et al. 2010), i.e., the mass index of the SFR-$M_\star$ relationship is less than unity. The SFR sequence has evolved by a factor 20 at a given stellar mass from $z \sim 2$ to the present time. This strong evolution of the SFR sequence implies that distant $z \sim 2$ SFGs with $M_\star > 10^{10.6} M_\odot$ had SFRs in excess of 100 $M_\odot\ {\rm yr}^{-1}$(Shapley et al. 2003; Erb et al. 2006a; Grazian et al. 2007; Daddi et al. 2007). Locally, such elevated SFRs are a natural outcome of merger-driven starbursts. However, the tightness of this relation, with rms scatter of less than 0.3 dex, indicates that SFR is not driven by merger-induced starbursts but rather by a continuous mass-dependent process that is gradually declining with time.

The mean mass dependence and time evolution of the relation between SFR and stellar mass can be summarized by the expression

$$\dot{M}_\star = 150\, M_{\star,11}^{p}\, (1+z)_{3.2}^{q}\, M_\odot\ {\rm yr}^{-1}\,, \qquad (1)$$

where $M_{\star,11} \equiv M_\star/10^{11} M_\odot$, $(1+z)_{3.2} \equiv (1+z)/3.2$, $p \simeq 0.8$, and $q \simeq 2.7$ in the redshift range $z = 0-2$. [6] Reproducing the characteristic mass and time dependencies of the SFR sequence is a challenge for models of galaxy formation (e.g. Davé 2008; Damen et al. 2009a).

Equation 1 is important as it is very reminiscent of the halo mean growth rate, which has been shown to be $\dot{M}_{\rm h} \propto {M_{\rm h}}^s (1+z)^t$ with a mass index s greater than unity $s \simeq 1.1$ (Neistein & Dekel 2008; Genel et al. 2008; McBride et al. 2009) that is set by the shape of the initial dark matter (DM) power spectrum (Neistein et al. 2006; Birnboim et al. 2007). The similarity motivates a closer investigation, and we will show that, indeed, there is a strong intimate connection between the growth of halos and the SFR sequence.

Another relevant scaling relation for (disky) SFGs is the well-known Tully-Fisher (e.g. Tully & Fisher 1977)

[1] Max Planck Institut für extraterrestrische Physik, Giessenbachstrasse, D-85748 Garching, Germany
[2] Department of Physics, University of California, Santa Barbara, CA 93106, USA
[3] Racah Institute of Physics, Hebrew University, Jerusalem, 91904, Israel
[4] Osservatorio Astrofisico di Arcetri, 50125 Florence, Italy
[5] Department of Astronomy, Campbell Hall, University of California, Berkeley, 94720 CA, USA

[6] There are marginal indications for a variation of p from near 0.7 at $z = 0-1$ (Brinchmann et al. 2004; Noeske et al. 2007a) to about 0.9 at $z \sim 2$ (Daddi et al. 2007; Santini et al. 2009; Pannella et al. 2009).

relation, which correlates stellar mass $M_\star$ and maximum circular velocity $V_{\rm max}$. The TF relation appears to be already in place at high-redshifts $z \geq 1$ (Kassin et al. 2007; Puech et al. 2008; Epinat et al. 2009; Cresci et al. 2009) and has evolved by a factor of 2.5 at a given mass (Cresci et al. 2009) from $z \simeq 2.2$ to the present. It is of the form:

$$M_\star \propto {V_{\rm max}}^m (1+z)^n, \quad (2)$$

where $m \simeq 4$ to a 10% accuracy locally (e.g. Tully & Pierce 2000; McGaugh 2005; Meyer et al. 2008). As for the SFR sequence, Equation 2 is reminiscent of the virial relation for DM halos, namely, $M_{\rm h} \propto V_{\rm h}^3$. Thus, both the SFR sequence and the TF relation behave similarly to their DM counterparts, but have slightly different mass indices, i.e., they are tilted with respect to their DM counterparts.

Aside from our knowledge on these global properties, our detailed understanding of individual SFGs has also improved greatly thanks to spatially resolved kinematic studies of the ionized gas in $z \sim 2$ SFGs (e.g. SINS survey, Förster Schreiber et al. 2006, 2009; Genzel et al. 2006, 2008; Shapiro et al. 2008, 2009; Cresci et al. 2009). The SINS survey, consisting of 80 $z = 2$ SFGs, has revealed that 30%–50% of SFGs with $M_\star \sim 10^{10.5-11.5}$ are gas-rich thick rotating disks (see also van Starkenburg et al. 2008; Wright et al. 2007), with the rest either dominated by dispersion velocities or showing the signature of recent mergers (e.g. Law et al. 2007, 2009; Förster Schreiber et al. 2009). The high-redshift SFG disks are different from local spirals in many ways. In particular, they are thick and correspondingly of high velocity dispersion (Förster Schreiber et al. 2006; Genzel et al. 2008; Cresci et al. 2009), and they are often made of giant SF 'clumps' (Cowie et al. 1995; Genzel et al. 2006; Elmegreen et al. 2007, Förster Schreiber, Shapley et al. in prep.). This feature indicates wild gravitational instability, which is a likely outcome of a high gas density (Noguchi 1998; Immeli et al. 2004; Bournaud et al. 2007; Elmegreen et al. 2008; Dekel et al. 2009b). Indeed, direct evidence for high gas fractions at high redshifts is now mounting (Erb et al. 2006b; Daddi et al. 2008; Tacconi et al. 2010; Daddi et al. 2010a) thanks to rapid progress in the sensitivity of mm interferometers.

The global scaling relations and the recent surveys of galaxy kinematics raise several outstanding questions: (1) What causes the high SFRs at $z \simeq 2$? (2) What drives the evolution of the SFR sequence and TF relation from $z \sim 2$ to the present? (3) What drives the cosmological evolution of the average SFR density? (4) Why did more massive galaxies form their stars before less massive SFGs? (5) Why are $z = 2$ SFGs so gas rich?

In this paper, we address these questions in the context of the cosmological growth of DM halos. In particular, we construct a very simple model that ties the SFR sequence and TF relation to their DM counterparts. The important feature of the model is the suppression of the accretion below a mass floor at $M_{\rm min} \sim 10^{11}\ M_\odot$, which, as we will show, has several other important consequences. We focus our attention at $z \simeq 2$, i.e., when the universe was just 3 Gyr old.

This paper is organized as follows. In Section 2, we present the model. In Section 3, we show that the SFGs reach a quasi-steady state and demonstrate the impact of the mass floor $M_{\rm min}$ on the SFR sequence and the TF relation. In Section 4, we find that the mass floor naturally delays the star-formation activity and leads to downsizing. The model also simultaneously accounts for the baryonic and gas fractions as a function of mass and time. In Section 5, we put direct constraints on the numerical value of $M_{\rm min}$ from the cosmological history of star-formation density. In Section 6, we discuss the model limitations and present our conclusions. Finally, in Section 7, we discuss the possible origin of the mass floor. We use throughout the standard ΛCDM cosmology with the parameters $\Omega_{\rm m} = 0.3$, $\Omega_\Lambda = 0.7$, $h = 0.7$ and $\sigma_8 = 0.8$.

2. THE RESERVOIR MODEL

In this Section we present our 'reservoir' model and its two major ingredients (Section 2.1), namely, the accretion efficiency, and the SF efficiency. We discuss the mass and redshift dependences of these two parameters in Section 2.2. The model ingredients are then summarized in Section 2.3. We will use this model as *a learning tool* to gain insights on the role played by several key physical parameters.

2.1. *The basic equation*

We consider a galaxy with its dark halo as a reservoir that is fed by a source and is emptied into a drain. The source represents the amount of newly accreted cold gas, and the drain is the gas consumption into stars as well as outflows. The basic equation of our model is the differential equation expressing the conservation of gas mass,

$$\dot{M}_{\rm gas} = \dot{M}_{\rm gas,in} - (1-R)\dot{M}_\star - \dot{M}_{\rm gas,out}\ , \quad (3)$$

where $\dot{M}_{\rm gas,in}$ is the gas accretion rate, $(1-R)\dot{M}_\star$ is the net SFR corrected for the recycled fraction, and $\dot{M}_{\rm gas,out}$ is the mass outflow rate. For our purposes, R is a kept time-independent given its slow dependence on stellar population age T for $T > 10^9$ Gyr (Bruzual & Charlot 2003), i.e., at $z < 4$. We discuss the limitations of this assumption in Appendix A.

To be as general as possible, we included an additional drain in our model (Equation 3) representing any outflowing gas. Observationally, the outflow rate $\dot{M}_{\rm gas,out}$ is observed to be roughly proportional to the SFR, $\dot{M}_{\rm gas,out} = a \times$ SFR, with $a \simeq 1.0$ (Heckman et al. 2000; Martin 2005; Rupke et al. 2005; Erb 2008). We note, however, that some fraction of the supernova (SN) driven winds is likely to be recycled, especially in the most massive halos, where much of the outflowing gas falls back into the galaxy and can boost the stellar mass at $z = 0$ by 33% (simulations by Oppenheimer & Davé 2008). Hence, the net outflow rate $\dot{M}_{\rm gas,out}$ may be less than the SFR, i.e., $\dot{M}_{\rm gas,out} \lesssim$ SFR.

Regardless of the numerical value of the proportionality constant a between outflow rate and SFR, Equation 3 can be re-written as

$$\dot{M}_{\rm gas} = \dot{M}_{\rm gas,in} - \alpha\dot{M}_\star\ , \quad (4)$$

where α includes the corrections for recycling and outflows. This equation expresses the trivial fact that

the gas reservoir $M_{\rm gas}$ will be filled up or get emptied depending on the relative power of the source and the drain terms. As discussed in section 3.1, the system will self-regulate itself to a steady state ($\dot{M}_{\rm gas} \simeq 0$) where SFR is proportional to the cosmological accretion rate.

We stress that the feedback term will have little impact on the scaling relations, such as the SFR sequence, or the sSFR. Indeed, if half of the accreting gas is entrained and expelled by the SN-driven winds, the SFR will be lowered by a factor of 2. As a result, if the SFR is lower by a factor of 2, the stellar mass $M_\star = \int {\rm dt\ SFR}(t)$ will be lower by the same factor, and the SFR sequence will remain unchanged.

2.1.1. *Halo growth and gas accretion*

The gas replenishment term $M_{\rm gas,in}$ in Equation 3 is required observationally. For example, the G-dwarf problem (van den Bergh 1962; Schmidt 1963) calls for a significant amount of newly accreted gas (e.g. Larson 1974). Furthermore, the gas depletion timescale in local massive galaxies is $\sim$ few Gyr (e.g. Wong & Blitz 2002; James et al. 2008), i.e., much shorter than the time required to build their stellar masses. Similarly, for $z \sim 2$ SFGs, the gas consumption timescale of less than 0.5 Gyr is shorter than their typical stellar ages of 1–2 Gyr (e.g. Erb 2008; Tacconi et al. 2010), thus requiring intense gas accretion.

Cold gas accretion is also required theoretically as it is a natural consequence of the 'cold-accretion' regime (Birnboim & Dekel 2003; Kereš et al. 2005) when the cooling time is shorter than the dynamical time (White & Frenk 1991). Furthermore, since the cold gas is not shock-heated to the virial temperature, high gas accretion efficiency is a natural outcome of efficient penetration of cosmological cold streams into the inner galaxies at high redshift, as seen in hydrodynamical cosmological simulations (Ocvirk et al. 2008; Dekel et al. 2009a).

In this context, it is the halo growth rate of DM halos that is regulating the baryonic accretion. The halo growth rate is by now well understood based on N-body simulations and the extended Press-Schechter (EPS) analytic formalism (Efstathiou et al. 1985; Wechsler et al. 2002; van den Bosch 2002; Springel et al. 2006). An approximation for the average mass growth rate of DM halos of virial mass $M_{\rm h}$ at redshift z in cosmological N-body simulations (van den Bosch 2002; Genel et al. 2008; McBride et al. 2009), which is also understood using the extended Press-Schechter (EPS) analytic formalism (Neistein & Dekel 2008), is obtained by the fitting function

$$\dot{M}_{\rm h} \simeq 510\, M_{\rm h,12}^{s} (1+z)_{3.2}^{t}\, M_\odot\ {\rm yr}^{-1}\,, \qquad (5)$$

where $M_{\rm h,12} \equiv M_{\rm h}/10^{12}\ M_\odot$, $(1+z)_{3.2} \equiv (1+z)/3.2$, $t \simeq 2.2$, and $s \simeq 1.1$, with the estimates for s ranging from 1.08 to 1.14 (Neistein & Dekel 2008; Genel et al. 2008; McBride et al. 2009)

Given the average halo growth rate, the corresponding average gas accretion rate is

$$\begin{aligned}\dot{M}_{\rm gas,in} &= \epsilon_{\rm in}\, f_{\rm b}\, \dot{M}_{\rm h} \\ &\simeq 90\, \epsilon_{\rm in}\, f_{\rm b,0.18}\, M_{\rm h,12}^{1.1}\, (1+z)_{3.2}^{2.2}\, M_\odot\ {\rm yr}^{-1}\,, \quad (6)\end{aligned}$$

where $f_{\rm b,18} \equiv f_{\rm b}/0.18$ is the cosmic baryonic fraction, and $\epsilon_{\rm in} \lesssim 1$ is the accretion efficiency expressing the effective fraction of the baryonic matter that is actually accreted as cold gas into the galaxy.

The accretion efficiency $\epsilon_{\rm in}$ is a very important parameter and must be within the range 0.5–1.0 for several reasons. Theoretically, $\epsilon_{\rm in}$ is high under the cold-accretion regime (Dekel et al. 2009a). Observationally, this efficiency is supported by the fact that the observed SFR in massive galaxies at $z \sim 2$ matches within a factor of two the maximum predicted gas accretion rate (Genel et al. 2008; Dekel et al. 2009a). In addition, Genel et al. (2008) showed that the halo major merger fraction in the mass range of interest $\log M_{\rm h} = 12$ is low and consistent with the low merger fractions in the SINS survey (Shapiro et al. 2008; Förster Schreiber et al. 2009), provided that the accretion efficiency $\epsilon_{\rm in}$ is greater than 50% (see Fig. 1 of Genel et al. 2008). Recently, Bauermeister et al. (2010) compared the inferred 'external' gas accretion to the DM accretion rate and found this efficiency needs to be $> 70\%$. In light of all these results, we will adopt a fiducial value of $\epsilon_{\rm in} = 0.7$.

As mentioned in the Introduction, this baryonic growth rate (Equation 6) is very reminiscent of the SFR-Mass relationship (Equation 1), given the similar near-linear increase of the accretion rate with mass. However, the mass index s in the accretion rate is slightly larger than unity, while the mass index p in the SFR sequence is somewhat smaller then unity. The clear implication from this difference is that the specific accretion rate increases with mass for the DM component, while the sSFR decreases with mass. Thus, if there is a connection between Equation 6 and Equation 1, the difference has to be explained (see Section 3).

2.1.2. *Star formation rate*

Star formation, a very complex, local and inefficient process (giant molecular clouds (GMCs) typically turning 1-2% of the gas mass into stars in a free-fall time) is the primary drain of the reservoir (in Equation 3). On galaxy scales, the amount of gas consumed is well described by the empirical relation:

$$\begin{aligned}\Sigma_{\rm SFR} &= \epsilon_{\rm sfr} \Sigma_{\rm gas}/t_{\rm dyn},\ \text{ i.e.,} \\ {\rm SFR} &= \epsilon_{\rm sfr} M_{\rm gas}/(t_{\rm dyn}), \qquad (7)\end{aligned}$$

where $t_{\rm dyn} = R_{1/2}/V_{\rm c}$ is the galaxy dynamical time, and $\epsilon_{\rm sfr}$ is the SFR efficiency parameter. For a marginally unstable disk with Toomre Q parameter $Q \sim 1$, it can be shown (Martin & Kennicutt 2001; Krumholz & Thompson 2007) that Equation 7 is equivalent to the traditional Kennicutt-Schmidt (KS) relation (Schmidt 1959; Kennicutt 1998), which relates the surface densities of gas and SFR via $\Sigma_{\rm SFR} \propto \Sigma_{\rm gas}^{1.5}$.

The locally inferred value by Kennicutt (1998) for the SFR efficiency is $\epsilon_{\rm sfr} \simeq 0.02$ and the most recent advancements in constraining the KS relation at $z \sim 2$ show no evidence for any evolution (Genzel et al. 2010; Daddi et al. 2010b). In addition, at $z \sim 2$, we know that massive disky SFGs, with $M_\star > 10^{10.5} M_\odot$, extend to half-light radii of $R_{1/2} \sim 4$ kpc (Bouché et al. 2007a) and they rotate with circular velocities $V_{\rm c}$ $\sim$200 km s^{-1} (Förster Schreiber et al.

2006). Expressing the quantities in these units, the orbital time can be written as

$$t_{\rm dyn} = 2\times10^7{\rm yr}\left(\frac{R_{1/2}}{4\,{\rm kpc}}\right)\left(\frac{V_{\rm c}}{200\,{\rm km\ s^{-1}}}\right)^{-1}. \quad (8)$$

At $z > 2$, we assume that the orbital time scales with the halo dynamical time, $R_{\rm vir}/V_{\rm h}$, which is a fixed fraction, about 18%, of the Hubble time at the given redshift, thus proportional to $(1+z)^{-3/2}$.

We note that our results on the scaling relations presented in 3.2 are completely independent of the SF efficiency (i.e., $\epsilon_{\rm sfr}$ and $t_{\rm dyn}$). This is because the SFR is going to be driven by the cosmological accretion rate, as explained in Section 3.1.

2.2. *Mass dependence*

The two efficiency parameters $\epsilon_{\rm sfr}$ and $\epsilon_{\rm in}$ appearing in Equations 6–7 may in principle vary with mass and redshift. The SF efficiency $\epsilon_{\rm sfr}$ does not appear to evolve with redshift. Indeed, the KS relation seems to be in place as early as $z = 2$ and shows no significant evolution between $z = 0$ and $z = 2$ (Bouché et al. 2007b).

On the other hand, the accretion efficiency $\epsilon_{\rm in}$ must be a strong function of halo mass (e.g. White & Frenk 1991). At the massive end $M_{\rm h} \gtrsim M_{\rm max} \simeq 10^{12} M_\odot$, and at low redshifts, the cold flows are not expected to be in a form of narrow, dense streams and they therefore fail to penetrate through the shock-heated halo gas. This may play a significant role in quenching star formation and causing the transition of blue galaxies onto the red sequence (Dekel & Birnboim 2006; Cattaneo et al. 2006). To model this effect, we set a ceiling for cold-gas accretion at all redshifts [7],

$$\epsilon_{\rm in}(M_{\rm h}) = 0 \ \text{ if } M_{\rm h} > M_{\rm max}. \quad (9)$$

At the low-mass end, there is strong evidence for a drop in the efficiency of galaxy formation (e.g. Shankar et al. 2006; van den Bosch et al. 2007; Baldry et al. 2008; Kravtsov 2010; Moster et al. 2010; Guo et al. 2010). In the spirit of our simple toy model approach, we make the ansatz,

$$\epsilon_{\rm in}(M_{\rm h}) = 0 \ \text{ if } M_{\rm h} < M_{\rm min}, \quad (10)$$

i.e., we set a sharp mass floor for $\epsilon_{\rm in}(M_{\rm h})$ below $M_{\rm min}$. For any reasonable physical mechanism that may be responsible for the suppression of accretion and SFR in low-mass halos (see Section 7), modeling the effect as a sharp cutoff is clearly a very crude approximation, but it is useful as a first attempt in capturing the key features with a minimum number of parameters.

This accretion floor means that the effective accretion of cold gas is suppressed in halos less massive than $M_{\rm min}$. Halos more massive than $M_{\rm min}$ accrete baryons that are embedded in other merging halos, which could themselves be more massive or less massive than $M_{\rm min}$, as well as smooth gas unbound to any halo (Stewart et al. 2008; Genel et al. 2010). The relative contribution of these different contributions leaves sufficient margins to meet an accretion efficiency of 0.7.

[7] Cold accretion can occur above this mass threshold at redshifts beyond $z = 2$ when the filament cross-section is much smaller than the virial radius. However, the number density of such halos with mass 10^{13} (and above) is low.

The accretion efficiency $\epsilon_{\rm in}$ at a given mass is likely to decline in time, as the overall fractions of stars and hot gas ($\gg 10^4$K) in the inter-galactic medium (IGM) grow. We model this by incorporating a redshift dependence $\epsilon_{\rm in}(z) = \epsilon_{\rm in}\ f(z)$, to allow for a decrease in cold accretion efficiency from $z = 2$ to $z = 0$. For simplicity reasons, we use a function linear in time with the boundary conditions $f(z = 2.2) = 1$ and $f(z = 0) = 0.5$. Note that our main results on the slope of the scaling relations are independent of this assumption since a change in $\epsilon_{\rm in}$ changes both SFR and $M_\star$ by the same amount. However, as we discuss in Section 3.4, this affects the evolution of the SFR sequence.

Figure 1(left) shows the mass growth histories for our modeled halos and the model accretion efficiency $\epsilon_{\rm in}(M_{\rm h})$ with the upper and lower cutoffs at $M_{\rm max}$ and $M_{\rm min}$. Figure 1(right) shows the maximum baryonic accretion rate $f_B\ \dot{M}_{\rm h}$ available for each halo as a function of time. More massive halos reach the $M_{\rm min}$ threshold first and cross $M_{\rm max}$ over a shorter time scale, leading to downsizing (see section 4.1).

2.3. *Overview of model ingredients*

At this stage, it is worth summarizing our model and its parameters. The model parameters are as follows:

1. The key assumption in our model is the halo mass floor for cold gas accretion $M_{\rm min}$, on the order of $10^{10} - 10^{11}\ M_\odot$. As we will show in Sections 3.2 and 5, $M_{\rm min} \simeq 10^{11}\ M_\odot$ will be required to match observations.

2. The halo mass ceiling for cold gas accretion $M_{\rm max}$, set at a value of $1.5\times10^{12}\,M_\odot$ to match the characteristic threshold for virial shock heating (Dekel & Birnboim 2006) and for best reproduction of the observed features of the galaxy bimodality (Cattaneo et al. 2006).

3. The cold gas accretion efficiency $\epsilon_{\rm in}(M_{\rm h}, z)$. As illustrated in Figure 1, it vanishes below $M_{\rm min}$ and above $M_{\rm max}$, and is set to 0.7 at $z > 2$. Below $z < 2$, we use $\epsilon_{\rm in}(z) = f(z)\times0.7$, where $f(z)$ is a function that is decreasing linearly with time with the boundary conditions $f(2.2) = 1$ and $f(0) = 0.5$.

4. The SFR efficiency $\epsilon_{\rm sfr} = 0.02$ set from the observed KS relation, and the orbital timescale $t_{\rm dyn} = 2\times10^7\ {\rm yr}\,(1+z)_{3.2}^{-1.5}$.

Our fiducial model described above is the "accretion floor" model, dubbed hereafter 'accFloor', where the accretion of cold gas, and therefore star formation, are totally suppressed below $M_{\rm min}$. We emphasize that our terminology 'accretion floor' means that the *effective* accretion of cold baryons is suppressed in halos with $M_{\rm h}(z) < M_{\rm min}$. Either these baryons are prevented from cooling or they are prevented from entering and reaching the central object.

In Section 3, we will analyze two radically different models for comparison (listed in Table 1): (1) in the other extreme 'noMmin' model, the mass floor is not applied at all, i.e., we allow both gas accretion and star formation to proceed unperturbed below $M_{\rm min}$ and (2) in the intermediate 'sfrFloor' model, we do allow gas

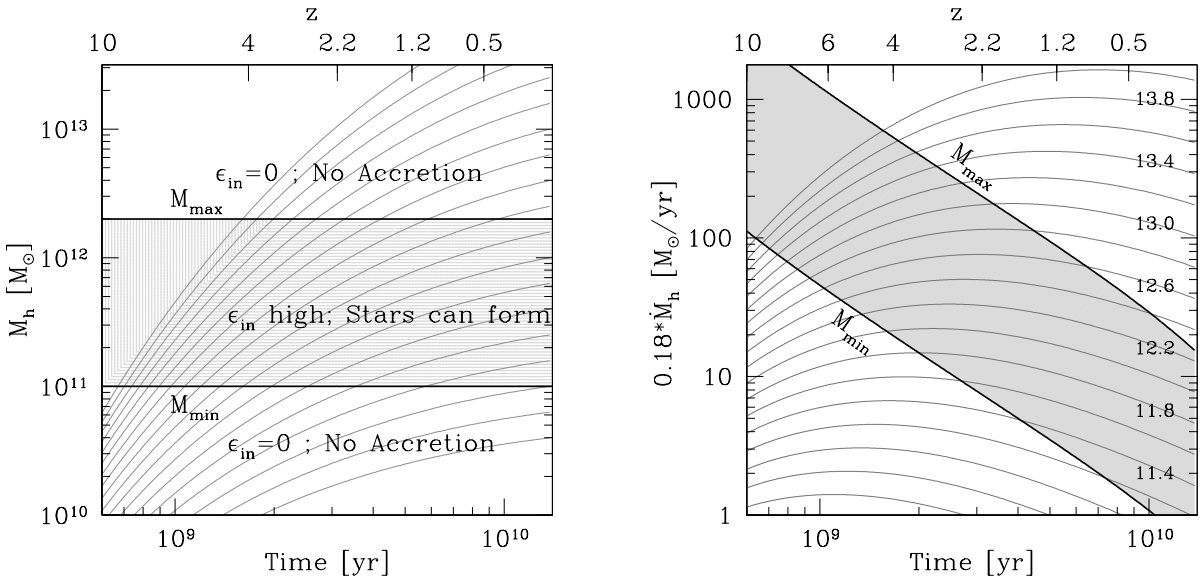

FIG. 1.— Left: The growth history $M_{\rm h}(z)$ for each modeled halo as a function of redshift calculated according to Equation 5. Above the quenching mass $M_{\rm max}$, accretion is increasingly hot. Below the quenching mass $M_{\rm max}$, cold accretion brings in gas efficiently with $\epsilon_{\rm in}$. Importantly, below a minimum mass $M_{\rm min}$, accretion is inefficient. Right: The maximum baryonic accretion rate inferred from the growth rate for each modeled halo. The final halo mass $M_{\rm h}(z=0)$ is labeled. More massive halos reach the $M_{\rm min}$ threshold first and cross $M_{\rm max}$ over a shorter time scale (downsizing; see Section 4.1).

Model	$M_{\rm max}$ $M_\odot$	$M_{\rm min}$ $M_\odot$	Floor	Feedback a
accFloor	1.5×10^{12}	10^{11}	accr.	0
noMmin	1.5×10^{12}	n.a.	n.a.	0
sfrFloor	1.5×10^{12}	10^{11}	sfr.	0
accFloor+	1.5×10^{12}	10^{11}	accr.	0.6

TABLE 1
DEFINITION OF OUR FIDUCIAL MODELS.

accretion below $M_{\rm min}$, but forbid star formation there. In this case, the cold gas accumulates until the halo becomes more massive than $M_{\rm min}$, and it then turns into stars. We also investigate the impact of the outflow term $\dot{M}_{\rm out}$ in Equation 3 with a model we term 'accFloor+'. However, as described in Section 2.1, this term will have no impact on the scaling relations.

Figure 2 highlights the main differences between the three alternative models, 'noMmin' (left), 'accFloor' (middle), and 'sfrFloor' (right). In the top panels, we show the assumed variation of $\epsilon_{\rm in}$ with redshift (thick solid lines, right axis) and the resultant evolution of the accretion rate (solid line), baryonic accretion rate (dashed line), and the SFR (dotted line) as a function of redshift. In the bottom panels, we show the resultant evolution of the DM halo mass (solid line), the maximum baryonic mass (dashed line), and the cold gas mass (dotted line). These three models differ significantly in their initial behavior. Compared to the 'noMmin' model, the 'accFloor' and 'sfrFloor' models add a (mass-dependent) delay in the evolution of SFR. In contrast to the 'accFloor' model, the 'sfrFloor' model accumulates cold gas till the halo reaches $M_{\rm min}$. Both of these models lead to no SF below $M_{\rm min}$, but have rather distinct physical interpretations and consequences.

2.4. *Numerical approach*

Using this simple reservoir set up (Equations 3 and 7), we solve for its gas and stellar content at each redshift as follows. We first construct average mass growth histories $M_{\rm h}(M_0, z)$ for the main progenitors of halos of masses in the range $M_0 = 10^{10.5-14}\ M_\odot$ today, as in Figure 1, following Neistein & Dekel (2008) (see their Equation8). We then numerically integrate Equations 3–7 for $M_{\rm gas}$ (and $\dot{M}_\star$) from $z=10$ to any z until $z=0$, with the initial conditions $M_{\rm gas} = M_\star = 0$ at $z=10$. The stellar mass $M_\star$ is updated at each time step according to $M_\star = (1-R)\int {\rm SFR\ dt}$, where $R=0.52$ is the recycled gas fraction for a Chabrier initial mass function (IMF) (Bruzual & Charlot 2003) [8].

3. RESULTS

3.1. *Steady state*

Before showing the numerical results, it is worth understanding the key behavior of the reservoir model from a qualitative inspection of Equations 3 and 7. When $M_{\rm gas}$ in the galaxy is still low, the SFR is low by the KS law (Equation 7), and it is smaller than the accretion rate dictated by the cosmological environment. The gas reservoir then gradually fills up until the SFR becomes comparable to the accretion rate (see Figure 3).

[8] For our purposes, R is a constant given its slow dependence on stellar population age T for age $T > 10^9$ Gyr.

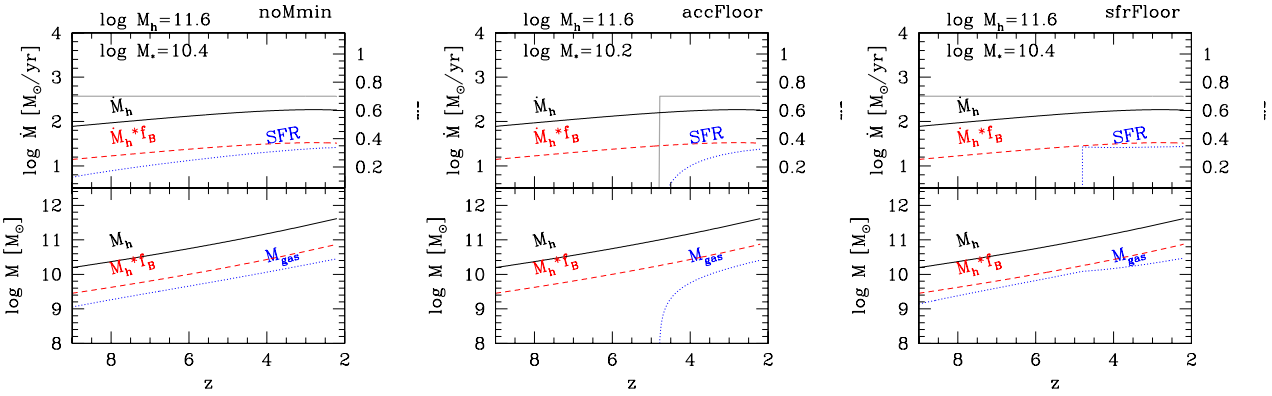

FIG. 2.— For a $\log M_{\rm h} = 11.6$ halo at $z = 2.2$, we show the behavior of each of our three models, namely when $M_{\rm min} = 0$ ('noMmin', left panel), when $\epsilon_{\rm in} = 0$ below the minimum mass floor ('accFloor', middle panel), and when $\epsilon_{\rm sfr} = 0$ below the SF floor $M_{\rm min}$ ('sfrFloor', right panel). The top panels show the redshift evolution of the DM accretion rate $\dot{M}_{\rm h}$ (solid line), the baryonic accretion rates ($\dot{M}_{\rm h} * f_B$) (dashed line) and the SFR (dotted line). The bottom panels show the halo mass ($M_{\rm h}$) (solid line), the maximum baryonic mass ($M_{\rm h} \times f_B$) (dashed line) and the gas mass ($M_{\rm g}$) (dotted line). The effect of $M_{\rm min}$ is clearly apparent in each case. The 'sfrFloor' model will lead to the same stellar mass $M_\star$ as the 'noMmin' model, given that the SF is simply delayed, and the amount of gas accreted remains the same.

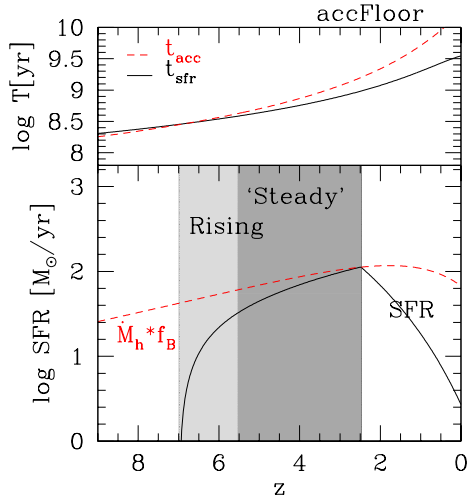

FIG. 3.— For our fiducial model ('accFloor'), the bottom panel shows the SFR (solid line) and the maximum accretion rate ($\epsilon_{\rm in}\ f_B \times \dot{M}_{\rm h}$) (dashed line). The top panel shows that below $z \simeq 5.5$, the accretion time scale ($t_{\rm acc} \equiv M_{\rm h}/\dot{M}_{\rm h}$) is longer than the SF time scale ($t_{\rm sfr} \equiv M_{\rm gas}/{\rm SFR}$). The reservoir model reaches rapidly a quasi-steady state in which the SFR scales with the accretion rate.

The galaxy enters a *quasi*-steady state where the SFR is essentially set by the accretion rate, SFR$\simeq \dot{M}_{\rm gas,in}$. Would the gas reservoir be temporarily overfilled (for its current SFR), the SFR would then be larger than the accretion rate, and the galaxy will return to the quasi-steady state.

Figure 3 demonstrates the quasi-steady state behavior. For our fiducial model ('accFloor'), the bottom panel shows the SFR (solid line) and the maximum accretion rate ($f_B\ \dot{M}_{\rm h}$) (dashed line). The reservoir model reaches rapidly a *quasi*-steady state in which the SFR scales with the accretion rate.

Because the accretion rate varies with redshift, the steady state can only be achieved when the timescale associated with SFR is comparable to or shorter than the accretion timescale. The SFR timescale, using Equation 8, is

$$t_{\rm sfr} \equiv \frac{M_{\rm gas}}{\dot{M}_\star} \simeq (t_{\rm dyn,7}/2)\ \epsilon^{-1}_{\rm sfr,0.02}\ (1+z)^{-1.5}_{3.2}\ {\rm Gyr}\,, \qquad (11)$$

where $t_{\rm orb,7} \equiv t_{\rm dyn}/10^7$ yr, and $\epsilon_{\rm sfr,0.02} \equiv \epsilon_{\rm sfr}/0.02$. From Equation 5, the accretion timescale is

$$t_{\rm acc} \equiv M_{\rm h}/\dot{M}_{\rm h} \simeq 2\ M^{-0.1}_{\rm h,12}\ (1+z)^{-2.2}_{3.2}{\rm Gyr}\,. \qquad (12)$$

Therefore, the condition that the SFR timescale be shorter than the accretion timescale

$$t_{\rm sfr} \leq t_{\rm acc} \qquad (13)$$

is met at redshifts $z \lesssim 7$.

The steady-state solution SFR$\propto \dot{M}_{\rm gas,in}$ has several important implications. First, it implies that the SFR(z) is driven by the (net) accretion rate as illustrated on Figure 3. As a result, at around $z \sim 2$, SFR maintains a high and slowly varying value for a few Gyrs (Figure 1(b)), which means that the average SFR is expected to be comparable to the instantaneous SFR. This is indeed supported by the SINS sample at $z \sim 2$, where the birthrate parameter, defined as the ratio of instantaneous to past SFR, is estimated to be $b \simeq 1.2$ (Förster Schreiber et al. 2009).

Second, the resulting SFR, gas and stellar masses are thus independent of the initial conditions given the rapid growth of the gas mass (see Figure 2).

Lastly, when the steady state condition (Equation13) is not met, the gas reservoir is being filled up at a rate faster than its consumption rate. In this case, SFR is time dependent, of the form t^a, and sSFR is proportional to $1/t$.

3.2. *Effect of $M_{\rm min}$ on scaling relations*

Our goal is to better understand the global scaling relations of $z \simeq 2.2$ SFGs, and the arguments presented in this Section are, however, applicable at $z = 0$, $z = 1$ as well. Thus, we take the naive point of view that

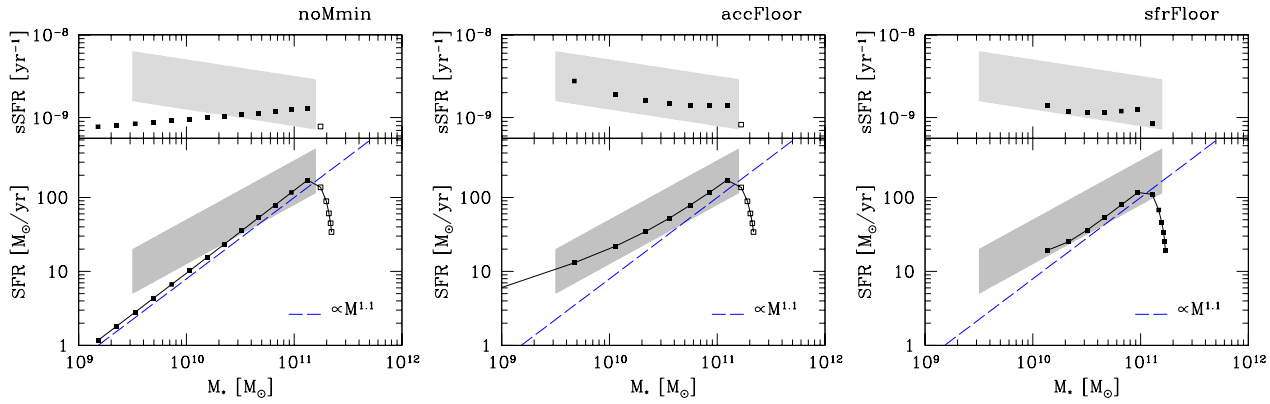

FIG. 4.— The $z = 2$ SFR sequence predicted from our three fiducial models with no mass floor $M_{\rm min}$ (left), an accretion floor (middle), and an SF floor (right). The modeled points are shown as filled (open) squares, for halos below (above) the virial shock mass $M_{\rm max}$. The observed SFR sequence from Pannella et al. (2009) and Daddi et al. (2007) is shown as gray shaded areas. The dotted line in each panel shows a line of slope 1.1 expected from the global accretion rate (Equation 5). The 'accFloor' model provides the best match to the observed SFR sequence with SFR$\propto M_\star^{0.8}$.

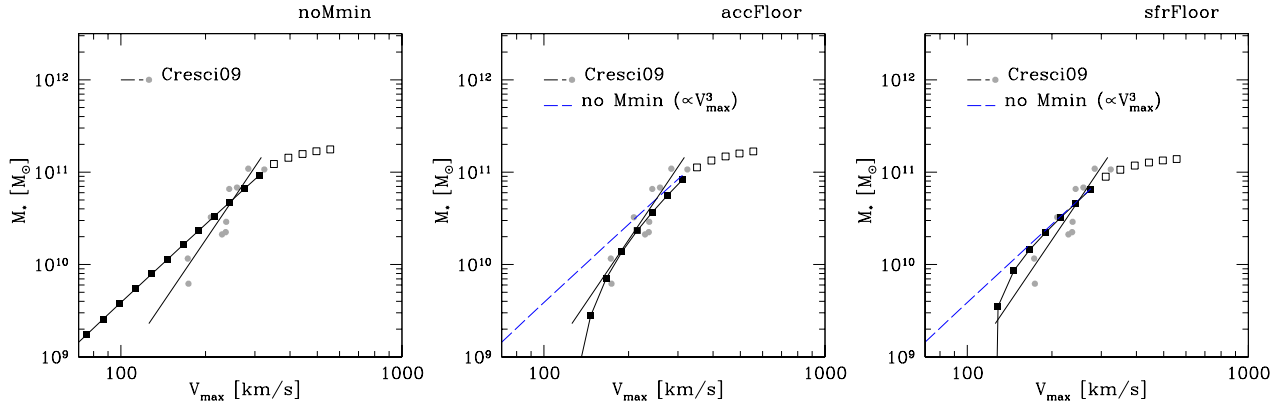

FIG. 5.— The $z = 2$ Tully-Fisher relation predicted from our simple model with no mass floor $M_{\rm min}$ (left), with an accretion floor (middle), and with an SF floor (right). The calculation for a model with no $M_{\rm min}$ is shown as dashed lines. The data from Cresci et al. (2009) are shown as gray circles. The 'accFloor' model provides the best match to the observed TF relation with $M_\star \propto V_{\rm max}^{\sim 4}$ (solid line).

the slopes of the scaling relations do not evolve with redshift and we stress that our aim is to demonstrate the key role played by the mass floor $M_{\rm min}$ in connecting the baryonic scaling relations to their DM counterparts. Any evolution in the slopes of the SFR sequence or TF relation will lead to an evolution of this mass floor.

Figure 4 shows the SFR sequence predicted by the three fiducial models ("noMmin", "accFloor" and "sfrFloor"), in comparison with the observed SFR sequence at that redshift from Pannella et al. (2009) and Daddi et al. (2007). The data show clearly that the sSFR is higher for lower mass galaxies (the mass index $p < 1$), whereas the expectation from the DM relation would predict an inverted trend since its mass index $s > 1$. The slope s =1.1 associated with the predicted accretion rate as a function of halo mass is shown as the dashed line. Figure 5 compares the corresponding $z = 2$ TF relation with the observed relation from Cresci et al. (2009). Similarly, the data show a tilt from the slope 3 associated with the virial relation $M_{\rm h} \propto V_{\rm h}^3$ (dashed line).

These two figures highlight our first significant results: the 'accFloor' model provides the best match to the two scaling relations. The mass floor $M_{\rm min}$ affects the slopes of both the SFR sequence and the TF relation in the right direction. It tilts the SFR sequence away from the 1.1 dark accretion rate, and steepens the TF relation away from the 3 virial slope. This effect can easily be explained.

When a mass floor is not applied, once the system reaches the steady state solution, SFR follows the halo accretion $\dot{M}_\star \propto \dot{M}_{\rm h}$ and thus scales with halo mass according to $\dot{M}_\star \propto {M_{\rm h}}^{1.1}$. Given that the halo mass is $M_{\rm h} = \int_0^t \dot{M}_{\rm h}\, {\rm d}t$, and that the stellar mass is $M_\star(t) \propto \int_0^t \dot{M}_\star\, {\rm d}t$, stellar mass and halo mass are proportional to each other: $M_\star \propto M_{\rm h}$. Hence, we expect in this case $\dot{M}_\star \propto M_\star^{1.1}$, as seen in the left panel of Figure 4.

When a mass floor for accretion is imposed (model accFloor), accretion (hence SF) is suppressed until the time $t_{\rm min}$ when the halo reaches $M_{\rm min}$, which is a decreasing function of $M_{\rm h}$, and thus of $M_\star$. The stellar mass is now an integral from $t_{\rm min}(M_{\rm h})$ to t: $M_\star(t) \propto \int_{t_{\rm min}}^t \dot{M}_\star\, dt$. The less massive systems had less time to grow stars and $M_\star$ is now smaller at a given halo mass, by a larger factor for a smaller halo. This effect is responsible for the required tilt both in the SFR sequence and the TF relation as seen in the middle panels of Figs. 4

and 5.

In the sfrFloor model, all the gas that has accumulated in the galaxy until $t_{\rm min}$ turns into stars after $t_{\rm min}$, so the total stellar mass after that time is expected to be the same as in model 'noMmin', as seen in the right panels of Figs. 4 and 5.

In summary, a mass-dependent delay in the gas accretion is found to be necessary to better reproduce the observed slopes of the scaling relations. In order for the time delay to have a significant effect, we find that $M_{\rm min}$ needs to be within 1 dex of $M_{\rm max}$, i.e., $M_{\rm min} \sim 10^{11}\ M_\odot$. In Section 5, we will put a stronger constraint on the numerical value of $M_{\rm min}$. The physical origin of the mass floor $M_{\rm min}$ is addressed in Section 7.

This mass-dependent delay can only be achieved in our model by the mass floor $M_{\rm min}$. Indeed, these results are completely independent of the SF efficiency $\epsilon_{\rm sfr}$ and of the feedback term in Equation 3. A change in these two parameters will lead to a change in both $M_\star$ and SFR, i.e., leaving the SFR sequence intact. A change in the accretion efficiency $\epsilon_{\rm in}$ via its mass dependence is the only mechanism that we found to affect the slope of the scaling relations.

3.3. *Connections between the two relations*

It is very interesting to realize that the TF relation and SFR sequence are in fact tied to each other. Indeed, the steady-state solution $\dot{M}_\star \propto {M_{\rm h}}^s$, together with the SFR sequence $\dot{M}_\star \propto M_\star^p$ implies the TF relation ($M_\star \propto V_{\rm h}^m$). Indeed, using the virial relation $M_{\rm h} \propto V_{\rm h}^3$, we find

$$m = 3s/p\,. \tag{14}$$

With the indices being $s \simeq 1.1$ and $p \simeq 0.8$, the TF slope is indeed $m \simeq 4$ as observed (e.g. Meyer et al. 2008; McGaugh 2005). Note that this argument holds for various values of the indices s and p as long as $s/p \simeq 4/3$. As noted in Section 1, there are marginal indications that p varies from near 0.7 at $z = 0-1$ (Brinchmann et al. 2004; Noeske et al. 2007a) to about 0.9 at $z \sim 2$ (Daddi et al. 2007; Santini et al. 2009; Pannella et al. 2009). These subtleties do not change our arguments given that all observational evidence show that $p < 1$ (sSFR higher at lower mass), while the DM counterpart has a mass index $s > 1$ (specific accretion rate higher at higher mass). Would this redshift dependence of the mass index p be confirmed, it would point toward a redshift evolution of $M_{\rm min}$.

Given that the slopes of these two scaling relations are coupled together and that, as we will show, the accretion rate regulates the evolution of the SFR sequence, we expect the accretion rate to regulate the evolution of the TF relation as well. However, a more detailed analysis of the TF zero-point normalization requires knowledge of the explicit relation between the virial velocity of the halo, which we crudely referred to so far as $V_{\rm h}$, and the observed maximum rotation velocity $V_{\rm max}$. Early models of galaxy formation assumed halo adiabatic contraction due to the infall of baryons into the halo center (Blumenthal et al. 1986; Mo et al. 1998), which gives typically $V_{\rm max} \simeq 1.6$–$1.8\,V_{\rm h}$ for a wide range of halo concentrations $c = [5, 30]$ and disk mass fractions $m_d = [0.02, 0.2]$. However, such models often fail to reproduce the observed TF zero point (e.g. Navarro & Steinmetz 2000; Dutton et al. 2007). Disk formation models can simultaneously fit the TF relation and the galaxy luminosity function if there was actually a slight halo expansion, where $V_{\rm max} \simeq 1.2\,V_{\rm h}$ (Dutton et al. 2007). Evidence against adiabatic contraction is mounting also at $z \sim 2$ (Burkert et al. 2010). We find that a similar factor of about 1.2 between $V_{\rm max}$ and $V_{\rm h}$ provides a good match to the TF zero point at $z \sim 2$.

3.4. *Redshift dependence*

According to Equation 1, the observed SFR-$M_\star$ relation (equivalently the sSFR) at a given stellar mass) is declining with time from $z = 2$ to the present by a factor ~ 20. Not only does our model reproduce this evolution, but it can help us understand its origin.

Figure 6(a) shows the model sSFR as a function of redshift for galaxies of different stellar masses, $M_\star = 10^{9.5}$, 10^{10} and $10^{10.5}\ M_\odot$, in comparison with observed sSFR for $M_\star$ in the range $10^{10} - 10^{10.5}\ M_\odot$ by Daddi et al. (2009); Damen et al. (2009a) and Pannella et al. (2009). One sees that our toy model reproduces the variation of sSFR with redshift relatively well to $z = 2$. We discuss the recent results at $z = 4$ to $z = 7$ in the Appendix.

The redshift dependence of the sSFR is driven by redshift evolution of the average accretion rate, Equation 5, which is $\propto (1+z)^{2.2}$. Simply put, this factor is driven by the expansion of the universe. This can be clearly seen using the EPS formalism, where the factor $(1+z)^{2.2}$ originates directly from the derivative of the linear growth factor $\dot{D}$ (Neistein & Dekel 2008; Birnboim et al. 2007). Indeed, under the EPS formalism, the specific accretion rate is $\dot{M}_{\rm h}/M_{\rm h} = -s(M_{\rm h})\dot{\omega}$, where $s(M_{\rm h})$ is the self-invariant mass variable, and $\omega(z) = 1.69/D(z)$ is the self-invariant time variable. $s(M_{\rm h})$ is a function of the variance of the initial density fluctuations on mass scale $M_{\rm h}$, $\sigma(M_{\rm h})$ (see Equation A5-A6 in Birnboim et al. 2007)

The dotted line in Figure 6(a) demonstrates that the time evolution of the sSFR (Equation 6) is indeed roughly proportional to $\dot{\omega}$, except that the predicted decline with time of the overall accretion rate is a bit slower than the decline in sSFR at $z < 1$ (Equation 1). An improved fit to the evolution at low redshifts is achieved by a small modification of the form $\dot{\omega} \times f(z)$ (long dashed line, defined in Section 2.3), attempting to correct for the gradual decline with time of the cold gas fraction in the overall baryonic accretion. This confirms that a gradual decrease in the accretion efficiency parameter, by a factor of ~ 2 between $z = 2$ and $z = 0$, helps recovering the observed evolution of the sSFR.

Davé (2008) parameterized the evolution of the SFR sequence at a given $M_\star$ in terms of a star-formation activity parameter, defined as $\alpha_{\rm sf} = (M_\star/\dot{M}_\star)/(t_H - 1{\rm Gyr})$. He pointed out that most models predict that galaxies have a growth rate comparable to t_H, the Hubble time, i.e., with a constant $\alpha_{\rm sfr} \simeq 1$, whereas observations reveal a growth of $\alpha_{\rm sf}$ by a factor of ~ 3 from $z = 2$ to $z = 0$ (see Fig 6). They used this apparent discrepancy to argue that the initial stellar mass function (IMF) must be evolving in time. Figure 6(b) shows the evolution of $\alpha_{\rm sf}$ predicted by our fiducial 'accFloor' model for

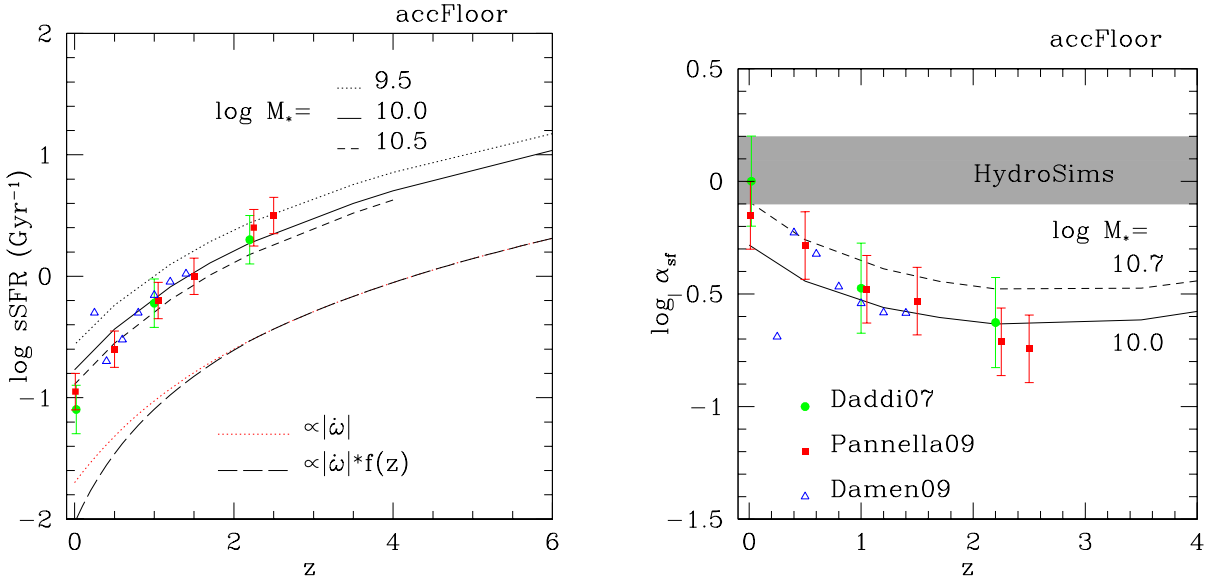

FIG. 6.— Left: Evolution of specific star formation rate (sSFR≡SFR/$M_\star$) at a fixed $M_\star$ from our fiducial model ('accFloor'). The dotted line shows the time dependence of the accretion rate through the function $\dot{\omega} \propto (1+z)^{2.2}$ (see text). The long-dashed line shows the slight modification of the introduced function $f(z)$ (defined in Section 2.3). Right: Evolution of the star formation activity parameter $\alpha_{\rm sf} \equiv (M_\star/\dot{M}_\star)/(t_H - 1{\rm Gyr})$. In both panels, we show the observations by Daddi et al. (2009) (solid circles), Damen et al. (2009a) (open triangles) and Pannella et al. (2009) (solid squares) for galaxies with $\log M_\star = 10$–10.5. The shaded area shows the hydrosimulation results of Davé (2008). The evolution of sSFR and $\alpha_{\rm sf}$ is mostly driven by the time dependence of the accretion.

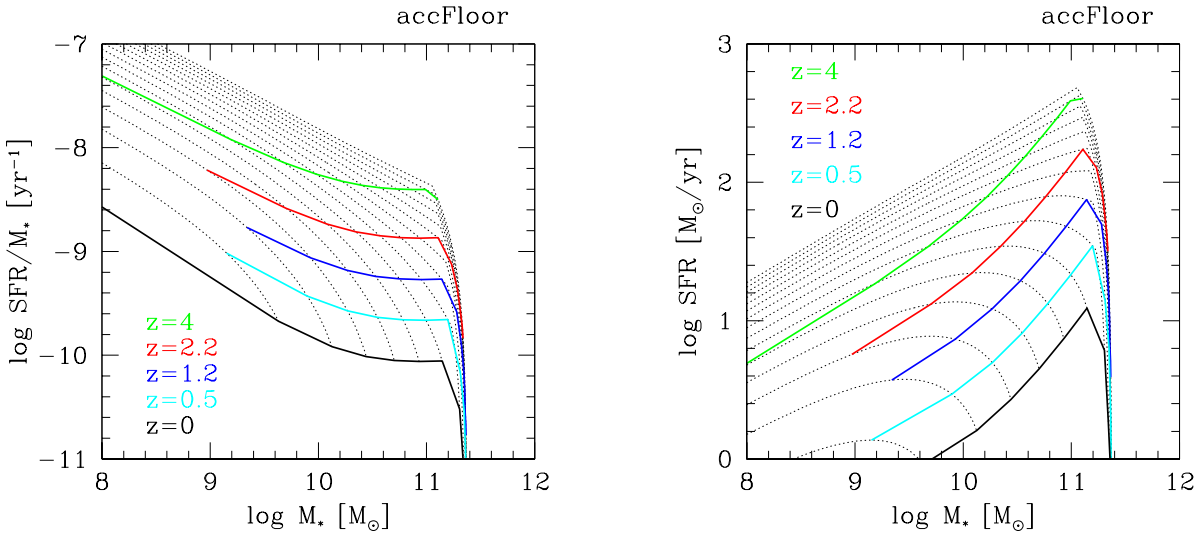

FIG. 7.— Left: Evolution of the sSFR-$M_\star$ relation. Right: Evolution of the main sequence. In both panels, the solid lines show the isochrones of the scaling relations at $z = 4, 2.2, 1.2$ and $z = 0$. The dotted lines show the individual tracks for the simulated halos.

$\log M_\star = 10.0$ and $10.7\,M_\odot$. An increase of $\alpha_{\rm sf}$ by a factor of ~ 3 between $z = 2$ and $z = 0$, not far from the observational result, without any evolution in the IMF, is a general feature of the time dependence of the accretion efficiency.

The SFR sequence and sSFR($M_\star$) at any given redshift are simply isochrones in their respective parameter plane. Our model gives us the opportunity to show the actual tracks of individual galaxies, which are shown in Figure 7 for the sSFR-$M_\star$ (left) and the SFR-$M_\star$ (right) relations.

4. ADDITIONAL ROLE OF $M_{\rm min}$

Given that our toy model seems to reproduce the scaling relations and their evolution rather well, we now compare the predictions of the model to observations involving the 'downsizing' effect (Section 4.1), the halo stellar fractions (Section 4.2), and the galaxy gas fractions (Section 4.3).

4.1. *Downsizing and tau models*

Stellar-population analyses of red galaxies in the local universe show that stars tend to have formed earlier and over a shorter time-span in the most massive ones (e.g. Heavens et al. 2004; Thomas et al. 2005; Jimenez et al.

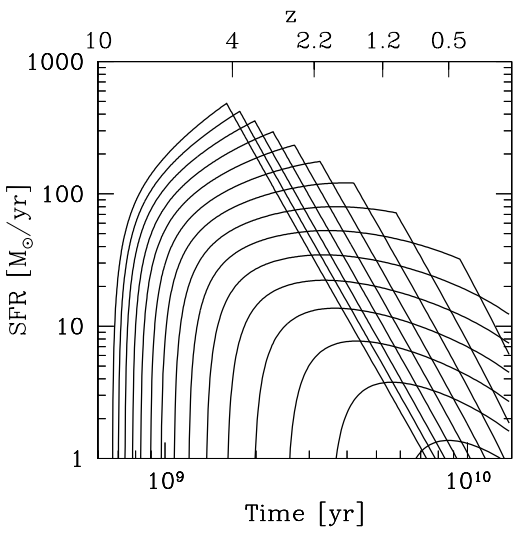

FIG. 8.— Star-formation history SFR(t) for our simulated halos of decreasing mass (from left to right). The individual tracks simply reflect that more massive halos reach the mass floor $M_{\rm min}$ earlier as shown in Figure 1 and form stars on a shorter time scale (before reaching the mass ceiling $M_{\rm max}$).

2007; Thomas et al. 2010). This is sometimes termed as 'archeological downsizing'. This age-mass correlation is also present in large samples (up to 3×10^5) of *active* galaxies in the Sloan Digital Sky Survey (SDSS) (e.g. Gallazzi et al. 2005; Jimenez et al. 2007).

The SF history (SFH) tracks shown in Figure 8 demonstrate the origin of the age-mass anti-correlation. More massive halos reach the mass floor earlier, and spend less time between the mass floor $M_{\rm min}$ and the mass ceiling $M_{\rm max}$. This is a natural consequence of the halo tracks in Figure 1 combined with our key assumption of $M_{\rm min}$.

Figure 9 shows the resulting age-mass relation at $z = 0$ (left) and $z = 2$ (right). The left panel shows the formation redshift z_f as a function of stellar mass. Similarly to Noeske et al. (2007b), the formation redshift z_f is defined here when star formation began, i.e., when $M_{\rm h}(z)$ reaches $M_{\rm min}$. The mass index of the resulting age-mass relation is surprisingly close to the $(1 + z_f) \propto M^{0.3}$ inferred by Noeske et al. (2007b) shown as the dashed line (normalization arbitrary).

That the SFR sequence leads to the same mass-dependent SFH as in the archeological downsizing was already argued by Noeske et al. (2007b). Indeed, they fitted τ-models to the $z \sim 1$ SFR-$M_\star$ relation and concluded the sSFR relation required both τ and the formation redshift z_f to be mass-dependent ($\tau \propto M^{-1}$, $(1 + z_f) \propto M^{0.3}$). They call this mass-dependent SFH 'Staged Galaxy Formation' where more massive galaxies are formed first on a shorter time scale. However, the mass dependency in our model did not have to agree with the results of Noeske et al. (2007a).

This age-mass relation may already be in place at $z \sim 2.2$ (Figure 9(right)). Indeed, the large sample of the SINS survey (Förster Schreiber et al. 2009) shows a similar trend between spectral energy distribution (SED) derived ages and stellar masses. In Figure 9, we compare these observations (gray points) to the luminosity weighted ages in our model (solid squares), which are derived according to $\int t_{\rm lbt} {\rm SFR}(t_{\rm lbt}) {\rm dt}_{\rm lbt}$ where $t_{\rm lbt}$ is the lookback time since $z = 2.2$.

Thus, our model reveals that the key player for downsizing is the accretion mass floor $M_{\rm min}$. As it was first realized in Neistein et al. (2006), the archeological downsizing effect is a direct consequence of a mass floor $M_{\rm min}$.

It has been noted that, for early type galaxies, the more massive ones reach the red sequence earlier, a phenomenon dubbed 'downsizing in mass' (Cimatti et al. 2006). In our model, when galaxies reach the ceiling mass $M_{\rm max}$, their gas supply dries out and SF is quenched, i.e., the galaxy becomes red and passive. The same SFH tracks shown in Figure 8 lead to this other type of downsizing, in this case due to $M_{\rm max}$ (see also Cattaneo et al. 2008).

4.2. *Stellar fractions*

Many have shown that the stellar fraction in galaxies is a strong function of the total halo mass (e.g. van den Bosch et al. 2003b; Eke et al. 2005; Shankar et al. 2006; van den Bosch et al. 2007; Kravtsov 2010; Moster et al. 2010; Guo et al. 2010) owing to the very different shapes of the halo mass function and the galaxy stellar mass function. We confront our toy model with this additional observational constraint.

Figure 10 compares the halo stellar fractions, defined as

$$f_\star \equiv \frac{M_\star}{0.18 * M_{\rm h}}\,, \qquad (15)$$

predicted from our model to relevant data at $z = 0$ (left) and $z = 2.2$ (right). The shaded area shows the results from the SDSS analysis of Guo et al. (2010), and the solid line shows the similar result from Moster et al. (2010). At $z = 2.2$, the observational estimates are from the disk-dominated galaxies of the SINS survey (Förster Schreiber et al. 2009; Cresci et al. 2009), where the virial mass is estimated assuming that $V_{\rm h} = V_{\rm max}$.

We see that the models 'noMmin' and 'sfrFloor' overpredict the stellar fraction for halos below $10^{12}\,M_\odot$, while the 'accFloor' model recovers the shape $f_\star(M_{\rm h})$, including the drop toward lower masses occurring at the proper range of $M_{\rm h}$. Once again, we learn that an effective halo mass floor for accretion at $M_{\rm min} \sim 10^{11}\,M_\odot$ is essential for a fit to the data.

However, the amplitude of the $f_\star(M_{\rm h})$ function predicted in the simple accFloor model needs to be reduced roughly by a factor two for a match with the data. A better fit is obtained if we include in our model (Equation 3) an outflow term

$$\dot{M}_{\rm out} = 0.6\,\dot{M}_\star.$$

This constraint is very consistent with the observations of Heckman et al. (2000) and Martin (2005) who found that $\dot{M}_{\rm out} \simeq$ SFR. Indeed, the corrections involved in deriving the outflow rates in galaxies (for ionization, metallicity, and depletion) are usually of several orders of magnitude. Moreover, the instantaneous outflow rate needs not be equal to our net outflow $\dot{M}_{\rm out}$ term, which only describes the baryons that leave the halo forever. We note that this constraint on the outflow rate is degenerate with the

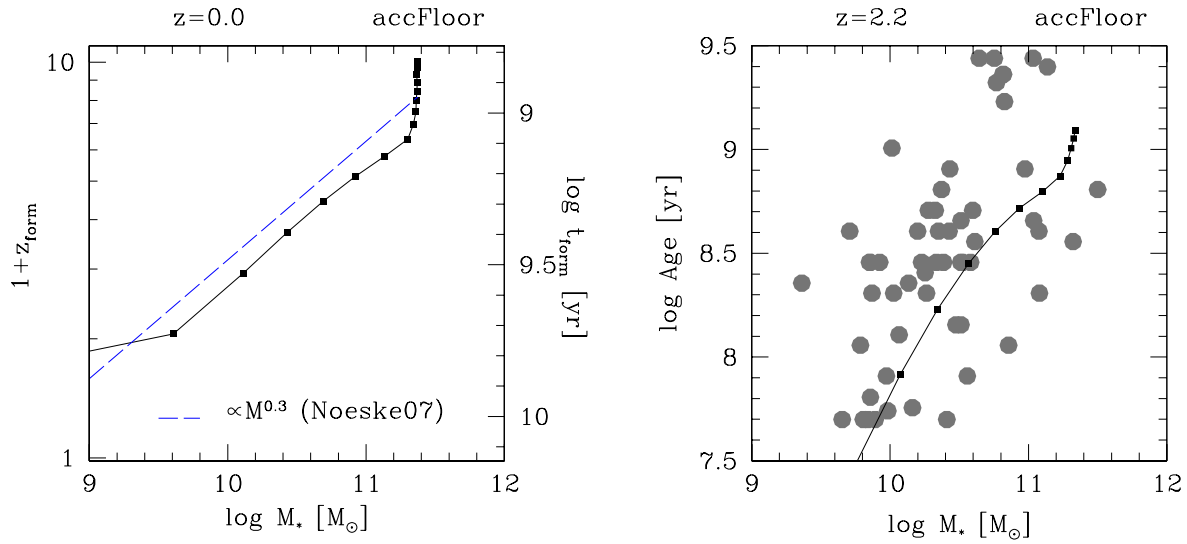

FIG. 9.— Archeological downsizing. Left: Formation redshift z_f (defined when $M_{\rm h}(z)$ reaches $M_{\rm min}$) as a function of stellar mass for our modeled galaxies (solid squares). The dashed line shows the $M_\star - z_f$ relation inferred by Noeske et al. (2007b) from the $z \sim 1.0$ SFR sequence, namely, $(1+z_f) \propto M_\star^{0.3}$ (normalization is arbitrary). Right: The modeled $z \sim 2.2$ age-$M_\star$ relation is shown with the solid squares. Modelled ages are the luminosity weighted ages (see text). The gray points show the ages (inferred from SED fitting) for the large sample of $z = 2$ SFGs available in the SINS survey (Förster Schreiber et al. 2009). At all epochs, the age-mass dependence is a direct consequence of the mass floor $M_{\rm min}$.

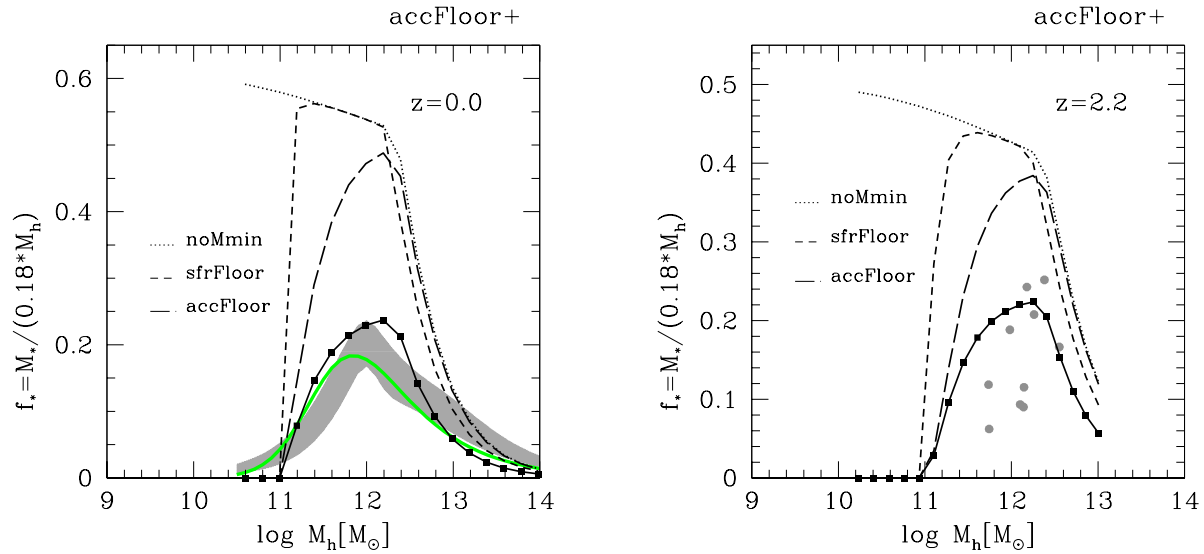

FIG. 10.— Stellar fractions ($f_\star \equiv M_\star/(0.18 * M_{\rm h})$) at $z = 0$ (left) and $z = 2$ (right) predicted from our fiducial model ('accFloor+'). In each panel, the alternative models, namely, with no mass floor $M_{\rm min}$ (dotted line), with an accretion floor (long dashed line), and with an SF floor (short dashed line) are indicated. The $z = 0$ stellar fractions from Moster et al. (2010) and Guo et al. (2010) are shown as the shaded area and thick line, respectively. The stellar fractions in $z = 2$ SFGs are shown as gray circles (Cresci et al. 2009).

accretion efficiency $\epsilon_{\rm in}$, i.e., $\dot{M}_{\rm out} = (0.4—0.8)\ \dot{M}_\star$ for $\epsilon_{\rm in}$ ranging from 0.5 to 1.0.

It is important to realize that the results presented thus far are independent of this outflow term. The SFR sequence is not sensitive to feedback as lowering the SFR by a factor of two leads to a stellar mass $M_\star$ lower by the same factor. Dutton et al. (2010) demonstrates this in a similar work.

4.3. *Gas fractions*

Another interesting constraint is provided by the gas fraction in galaxies, defined as

$$f_{\rm g} \equiv \frac{M_{\rm g}}{M_{\rm g} + M_\star}\,. \tag{16}$$

At low redshift, we learn from all-sky HI surveys (e.g. Zwaan & et al. 2003; Rosenberg & Schneider 2003; Meyer et al. 2004; Giovanelli et al. 2005; Wong et al. 2006; Catinella et al. 2010) that the gas fractions in SFGs vary systematically with stellar mass (e.g. Baldry et al.

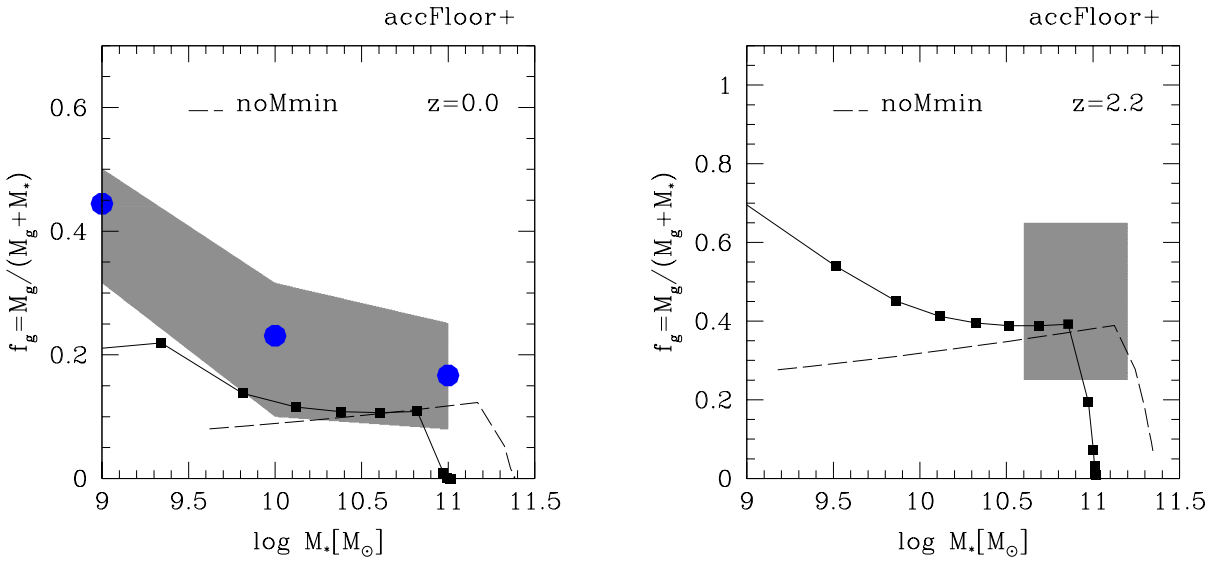

FIG. 11.— The solid squares show the gas fractions as a function of $M_\star$ predicted from our fiducial model 'accFloor+' at $z = 0$ (left) and $z = 2$ (right). The observed local gas fractions from Baldry et al. (2008) and Zhang et al. (2009) are shown as the solid circles and shaded area, respectively. The new $z \sim 2$ gas fraction is represented by the shaded box for dozen SF galaxies with $\log M_* > 10.6$ (see Tacconi et al. 2010). The upturn of f_g at the low mass end is again a result of the mass floor $M_{\rm min}$.

2008, and references therein). These data are presented in the left panel of Figure 11. At $z \sim 2$, thanks to the rapid progress in the sensitivity of millimeter interferometers (such as the IRAM Plateau de Bure interferometer, PdBI), it is now possible to study CO rotational emission lines of normal high redshift SFGs at $z > 1$ and therefore constrain their gas masses. The observed gas fraction for $z \sim 1$–2.5 SFGs with $M_\star > 10^{10.6}\,M_\odot$ ranges from 0.3 to 0.6 (Daddi et al. 2010a; Tacconi et al. 2010) with an average of about 0.44 for the large sample of 19 SFGs of Tacconi et al. (2010).

Figure 11 compares the predicted $f_{\rm g}(M_\star)$ from our model 'accFloor+' to those observations at $z = 0$ (left) and $z = 2$ (right). We see that the model is consistent with the data both at $z = 0$ and at $z \sim 2$. Locally, the upturn of f_g at the low mass end is again a result of the mass floor $M_{\rm min}$.

Contrary to the other results presented so far, the gas fractions are sensitive to SF efficiency $\epsilon_{\rm sfr}$, given that the SFR is set by the steady-state solution (or by the accretion rate). A lower SF efficiency leads to higher gas fractions and vice-versa. We used a universal $\epsilon_{\rm sfr}$ set by the KS relation and the redshift evolution of f_g in our model appears to be very consistent with observations. Indeed, the model predicts $f_{\rm g} = 0.4 - 0.55$ at $z = 2$ and $f_{\rm g} = 0.3 - 0.45$ at $z = 1$, which is in good agreement with the average gas fractions estimated from the CO observations, 0.44 and 0.34, respectively (Tacconi et al. 2010, see also Daddi et al. 2010).

Our simplistic toy model, which was only tuned (with $M_{\rm min}$) to reproduce the scaling relations, helps us also to understand the trends of gas fraction with mass and redshift for SFGs.

5. STAR-FORMATION HISTORY: CONSTRAINING THE MASS FLOOR

Thus, based on the two scaling relations, the stellar and gas fractions, our model shows that a mass floor $M_{\rm min}$ must play an important role in galaxy formation and we argued that $M_{\rm min}$ should be $\sim 10^{11}\ M_\odot$. We are about to show that the evolution of the average density of SF, $\dot\rho_\star(z)$, will give us a quantitative constraint on $M_{\rm min}$.

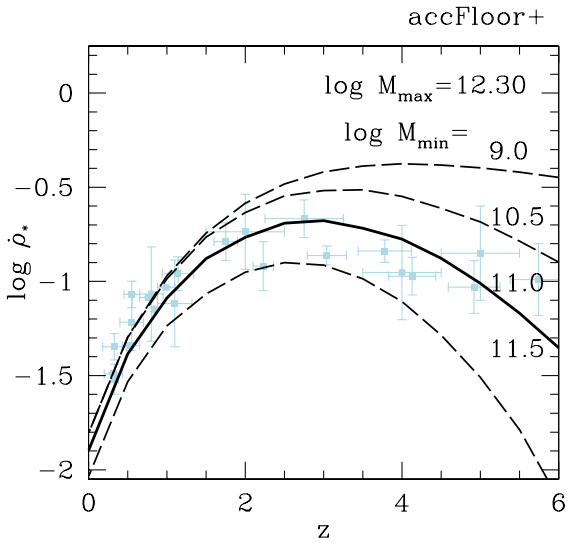

FIG. 12.— The star formation history $\dot\rho_\star$. The dashed curves show that $\dot\rho_\star(z)$ is very sensitive to the minimum mass $M_{\rm min}$. The light symbols show the most recent $z < 2$ observations (Schiminovich et al. 2005; Dahlen et al. 2007; Mobasher et al. 2009) with the $z > 2$ data (Hopkins & Beacom 2006; Verma et al. 2007; Wilkins et al. 2008) all converted to a Chabrier IMF following Hopkins & Beacom (2008).

Figure 12 shows a compilation of data for the cosmic SFH, derived from observations under the assumption of a Chabrier IMF. The average density of SF, $\dot\rho_\star$, is observed to be rising from $z \sim 6$ to $z \sim 2$, reaching a plateau at about $z \sim 2$, and then dropping by an order of magnitude between $z \sim 1$ and $z = 0$ (e.g. Lilly et al.

1996; Madau et al. 1996; Hopkins & Beacom 2006, and references therein).

Our 'accFloor+' model convolved with the Sheth-Tormen model for the halo mass function (Sheth et al. 2001) is shown for 4 different values of $M_{\rm min}$, ranging from 10^9 to $3\times10^{11}\,M_\odot$. We see that the value of $M_{\rm min}$ indeed determines the growth of $\dot\rho_\star$ with time at high redshift. Best agreement to the growth rate observed at $z>2$ is obtained with $M_{\rm min}=10^{11}\,M_\odot$. Thus, we conclude that the rise in the cosmic SFH from $z=6$ to $z\sim2$ confirms the necessity of a mass floor and provides the strongest constraint on the value of $M_{\rm min}$.

Our model can also help us to understand the origin of the decline at late times. Possible reasons for this sharp decline could in principle be the acceleration of the universe at recent cosmological epochs, gas exhaustion into stars and outflows, the quenching of SFR above the mass ceiling, or simply the generic decline in the accretion rate into dark-matter halos due to the expansion of the universe. The sharp decline at $z<2$ is predominantly driven by the decreasing accretion rate as a direct result of the expansion of the universe as it can be seen from Figure 1 (right) and discussed in Section 3.4. All the other potential sources for the decline, including the acceleration of the universe and the introduction of $M_{\rm max}$ or gas consumption, have only minor effects on this decline.

Many other groups (e.g. Springel & Hernquist 2003; Nagamine et al. 2006; Schaye et al. 2010; Choi & Nagamine 2009) have used cosmological hydrosimulations to investigate the cosmic SFH and to identify the physical processes that drive its evolution. Similarly to our model, Hernquist & Springel (2003) used an analytical approach and reach similar conclusions. They find that, at high-z, the rise in $\dot\rho_\star(t)$ originates from the gravitationally driven growth of halos, while at low-z, the decline is due to the expansion of the universe, through the inhibition of cooling. While in our model the SFR at a given halo mass is driven by the halo growth rate, their model assumes an ad-hoc form for the sSFR that is constant as a function of mass for all halos of virial temperature above 10^4 K. Similarly to our $M_{\rm min}$ assumption, in their model, stars do not form in halos below $T_{\rm vir}=10^4$ K. Their assumption also leads to a peak in the SFH, albeit at a higher redshift $z\sim5$ or 6. In spite of the differences between their results and our results, this again illustrates the impact of a mass floor.

6. DISCUSSION AND CONCLUSIONS

The purpose of this paper is to seek a basic understanding of the relations between global properties of SFGs and their time evolution between $z\sim2$ and today. This includes the origin of the SFR sequence and the Tully-Fisher relation. We achieved this via an idealized and remarkably simple 'toy' model, based on the cosmological evolution of accretion rate into dark-matter halos, the efficient deep penetration of cold gas streams into the central galaxies and the standard efficiency of SFR in galactic disks. The model should be interpreted as a learning tool for gaining insight into the role played by several key physical processes.

The model naturally leads to the observed scaling relations, $\dot M_\star\propto M_\star^{0.8}$ and $M_\star\propto V_{\rm max}^4$ and to the archeological 'downsizing' phenomenon, *provided* that there is a mass floor $M_{\rm min}\sim10^{11}\,M_\odot$ below which the accretion of cold gas is substantially suppressed [9]. An analysis of the SFH allowed us to put an additional strong constraint on the mass floor: $M_{\rm min}\simeq10^{11}\,M_\odot$, corresponding to $V_{\rm h}\sim100\,M_{\rm h,11}^{1/3}\,(1+z)_{3.2}^{1/2}$km s^{-1}, best accounts for the observed scaling relations.

Recently, Dutton et al. (2010) have used full semi-analytical approach to study the origin of the SFR sequence. While we agree with the conclusions of Dutton et al. (2010) with respect to the steady state, the impact of feedback, and to the evolution of the SFR sequence, our model differs from theirs on one significant aspect: the lack of a mass floor. Cattaneo et al. (2010) used a full semi-analytical model with an effective efficiency $\epsilon_{\rm in}$ similar to ours (compare their Fig.4 to our Fig.1). Their effective mass floor is due to the combined effect of SN feedback and photo-heating due to reionization. These authors, however, used a re-ionization threshold at $V_{\rm re}=40$ km s^{-1} in order to fit the luminosity function, which is higher than expected ($V_{\rm re}\sim10$ km s^{-1}) from pure reionization (e.g. Barkana & Loeb 1999; Iliev et al. 2005) by an order of magnitude in halo mass.

6.1. *Caveats and limitations*

Our model, which relies mainly on the cosmological accretion rate, is based on very few parameters ($\epsilon_{\rm in}$, $M_{\rm max}$, and $M_{\rm min}$) compared to semi-analytic models (e.g. Somerville et al. 2008). Our main free parameter is $M_{\rm min}$ (affecting the cooling/accretion efficiency $\epsilon_{\rm in}(M)$), as we use normal a SF efficiency $\epsilon_{\rm sfr}$ and set $M_{\rm max}$ following Cattaneo et al. (e.g. 2006, 2008).

The remarkably few parameters in our model are clearly an advantage (see also Neistein & Weinmann 2009), but this inevitably leads to over-simplifications. For instance, modeling the lower and upper thresholds for cold gas accretion as sharp cutoffs is clearly unphysical. In reality, these transitions are likely to be smooth and to depend on other galaxy properties. For example, $M_{\rm max}$ is rather sensitive to the metallicity in the halo (Dekel & Birnboim 2006). Indeed, the smoothness of this transition near $M_{\rm max}$ can be derived from hydrodynamical simulations (Kereš et al. 2005; Birnboim et al. 2007; Ocvirk et al. 2008; Kereš et al. 2009). In fact, a smooth transition at $M_{\rm max}$ would relieve the tension between the model and the observed scaling relations at the massive end, $M_*\sim10^{11}\,M_\odot$, in Figures 4 and 5.

The toy model presented in this paper does not allow us to address other observational constraints such as the mass-metallicity relation because this is rather sensitive to the exact treatment of the metal content of the stellar, SN outflows combined with the unknown fraction of ISM that is entrained in the outlow.

We also cannot address the scatter in the scaling relations as the model deals only with the mean global properties. Variations in the mass assembly history are to be expected (e.g. Genel et al. 2008) and will likely

[9] We note that the threshold could have been defined in terms of a constant virial velocity $V_{\rm h}$, and this would have lead to similar results.

contribute to the scatter in the scaling relations (e.g. Dutton et al. 2010).

Another limitation of our simplified model is that we do not include bulge growth, which can be an additional drain for SF disks in our model.

6.2. *Conclusions*

In spite of its simplistic assumptions, our model captures many of the observed properties of SF galaxies and their evolution. This approach helps us gain insight into the following questions:

• *Why are the $z = 2$ SFRs so high? What sets the SFR sequence?* Once the timescale for SF becomes shorter than the accretion timescale, galaxies settle in a quasi-steady state where the SFR is driven by the accretion rate (Figure 3). As a consequence, the high SFRs for $z = 2$ SFGs are driven by the high accretion rate of cold baryons. The steady state also implies that the instantaneous SFR is comparable to the average SFR ($\langle$SFR$\rangle$) for a few Gyr from $z \sim 4$ to $z \sim 1.5$ (see Figure 1(b)). This is consistent with observations from the SINS survey (Förster Schreiber et al. 2009) where the ratio $\langle$SFR$\rangle$/SFR is found to be $\simeq 1.0$ in $z = 2$ SFGs.

• *What is the origin of the scaling relations of SFGs?* We find that a single parameter, namely, the mass floor $M_{\rm min} \sim 10^{11} M_\odot$ for accretion, is key in generating the correct slopes of both the SFR sequence and the TF relation (Figs. 4 and 5). Thus, the two scaling relations are not independent relations, as we show in Section 3.3.

We emphasize that the SFR sequence and its evolution are insensitive to the values of the efficiency parameters $\epsilon_{\rm in}$ and $\epsilon_{\rm sfr}$, because changes in either of these efficiencies affect both $\dot{M}_\star$ and $M_\star$, and shift galaxies along the SFR sequence. The same argument holds for the impact of feedback on the SFR sequence (see Dutton et al. 2010). This is the reason for the failure of any model that attempts to reproduce the tilts of the scaling relation by varying either the SF efficiency or the feedback efficiency (see Davé 2008; Damen et al. 2009a, and references therein).

• *What sets the evolution of the SFR-$M_\star$ relation?* The redshift evolution of the SFR sequence (or sSFR) is driven predominantly by the redshift evolution of the cosmological DM accretion rate. Both the SFR sequence and the sSFR at a fixed mass follow the cosmological decline of average accretion rate onto halos as a result of the expansion of the universe (Figure 6). A slight improved match with the observations is obtained when we force the accretion efficiency to decrease with time at $z < 2$.

• *What is the origin of archeological downsizing?* Why did more massive galaxies form their stars earlier and over a shorter duration (e.g. Heavens et al. 2004; Thomas et al. 2005; Gallazzi et al. 2005; Jimenez et al. 2007)? An inspection of the halo trajectories in (Figure 1) reveals that more massive halos reach the mass floor earlier, and spend less time between the mass floor and the mass ceiling (see also Figure 8). It is the mass floor $M_{\rm min}$ that naturally produces the age-mass relation (Figure 9) as Neistein et al. (2006) already pointed out.

• *Is the observed low stellar fraction compatible with the high accretion efficiency of cold gas?* Having a high accretion efficiencies ($\epsilon_{\rm in} > 50\%$) is entirely compatible with the observed stellar mass fractions $f_\star$ that are low ($< 50\%$), i.e., $f_\star \sim 0.20$ (Figure 10) provided a net outflow rate $M_{\rm out} \propto 0.6\,\dot{M}_\star$ is included. This is consistent with observations $M_{\rm out} \simeq 1.0\,\dot{M}_\star$ given that a significant fraction of the out-flowing gas may be returned into the interstellar medium by $z = 0$ (e.g. Oppenheimer & Davé 2008);

• *Why are the gas fractions large at $z > 1$?* The observed high gas fractions at > 1 arise naturally from the high, mass-dependent accretion efficiency and the low star-formation efficiency. The SFR is set by the accretion rate in the steady-state solution, while the gas fraction is determined by the SFR efficiency $\epsilon_{\rm sfr}$. The model predicts mean gas fractions of 30%–45% at $z = 1.2$ and 40%–55% at $z = 2.2$ (Figure 11) in good agreement with the recent observations of Tacconi et al. (2010) and Daddi et al. (2010a).

• *What is the origin of the shape of the SFH?* The decline in the SFH from $z = 2$ to the present is primordially due to the decline in accretion rate associated with the cosmological expansion. The rise of $\dot{\rho}_\star$ from $z = 6$ to $z = 2$ necessitate a mass floor near $M_{\rm min} \sim 10^{11}\,M_\odot$ (Figure 12).

The successes of our model are evidence for the central role played by the key ingredient of our reservoir model, namely, the halo growth rate in the standard cosmology. While our model reveals the importance of a mass floor $M_{\rm min}$ for accretion, it does not address its physical origin.

7. ON THE ORIGIN OF THE MASS FLOOR

The exact mechanism that suppresses or holds accretion below $M_{\rm min}$ may be due either to photo-heating associated with the fresh UV background after reionization (e.g. Thoul & Weinberg 1996; Quinn et al. 1996; Barkana & Loeb 1999; Gnedin 2000; Dijkstra et al. 2004), or to SN feedback (e.g. Dekel & Silk 1986; Dutton & van den Bosch 2009; Oppenheimer & Davé 2008) [10]. Photo-heating associated with re-ionization increases the mean temperature of the IGM to $\sim 10^4$ K. This reduces the cooling rate of the hot gas and prevents the assembly of new low-mass galaxies with $V_{\rm h} < 10$km s^{-1}(or $M_{\rm h} \sim 10^8 M_\odot$), and those that have already collapsed are relatively quickly photo-evaporated (e.g. Barkana & Loeb 1999; Iliev et al. 2005). SN explosions, like photo-heating from reionization, provide a negative feedback on SF. If present simultaneously, photo-heating and SN feedback effects can mutually amplify each others ability to suppress the SFR (Pieri & Martel 2007; Pawlik & Schaye 2009). Lastly, the formation of cold ($T \sim 10$–30 K) molecular gas (necessary for SF) requires specific physical conditions in addition to high gas densities, such as high gas pressure (Blitz & Rosolowsky 2006) and pre-enrichment. Whether these conditions are met in low mass halos is an open question. Furthermore, radiative feedback effects from massive stars during intense SF episodes could play a crucial role in disrupting the GMCs as proposed by Murray et al. (2010).

[10] Note, in the context of momentum driven winds (Oppenheimer & Davé 2008), our mass floor corresponds to a threshold in the mass loading factor η where $\eta \to \infty$ below $M_{\rm min}$.

It is possible that no single mechanism can produce such a mass floor. For instance, since simple arguments on SN feedback give $f_\star \propto M_\star/M_{\rm h} \propto {M_{\rm h}}^\beta$ with $\beta = 2/3$ (Dekel & Silk 1986), an additional physical process must be at play. The combination of SN feedback and a (very high) reionization threshold can produce a steeper $f_\star$ as shown in Cattaneo et al. (2010). Similarly, van den Bosch et al. (2003a) and Mo et al. (2005) showed that artificially induced re-heating of the IGM to $T \sim 10^5$ K directly leads to a mass-dependent efficiency $f_\star$. However, this effects alone also cannot account for the steep mass dependence of $f_\star$ (e.g. Lu & Mo 2007).

Lastly, Cantalupo (2010) argued that the missing ingredient could be the effect of photoionization by local sources on the incoming cooling gas. He showed that soft X-ray generated by SF efficiently alters the ionization state of atoms, such as O. This effectively removes the main coolants and increases the cooling times by orders of magnitude, essentially stopping accretion, preferentially in low-mass halos. While this is an attractive mechanism, further work is needed in order to understand quantitatively whether photo-ionization from local sources are able to regulate the cosmological gas accretion rates.

One way to gain insight into which of these possible mechanisms are at play is to constrain the transition in accretion efficiency near $M_{\rm min}$ ($\epsilon_{\rm in} \propto {M_{\rm h}}^\eta$), which is related to the slope β of the relation $f_\star \propto M_\star/M_{\rm h} \propto {M_{\rm h}}^\beta$ under the quasi-steady state solution with $\eta \sim \beta$. Our modelling indicates that η should be steeper than unity. Observationally, various groups have determined that β is ≥ 2 (Shankar et al. 2006; Baldry et al. 2008; Kravtsov 2010; Moster et al. 2010; Guo et al. 2010).

We thank the anonymous referee for his or her constructive report. We specially thank A. Renzini for stimulating comments on a earlier draft that have led to significant improvements. We also thank D. Schaerer and K. Finlator for useful discussions. This research has been supported by the German-Israeli Foundation (GIF) grant I-895-207.7/2005, by the German Research Foundation (DFG) via German-Israeli Project Cooperation grant STE1869/1-1.GE625/15-1, and by a grant from the Israel Science Foundation. N.B. acknowledges the hospitality at the Racah Institute of Physics of the Hebrew University of Jerusalem where much of this work has been performed. N.M.F.S. acknowledges support from the Minerva Program of the Max-Planck-Gesellschaft.

REFERENCES

Baldry, I. K., Glazebrook, K., & Driver, S. P. 2008, MNRAS, 388, 945
Barkana, R., & Loeb, A. 1999, ApJ, 523, 54
Bauermeister, A., Blitz, L., & Ma, C. 2010, ApJ, 717, 323
Bell, E. F. et al. 2005, ApJ, 625, 23
Birnboim, Y., & Dekel, A. 2003, MNRAS, 345, 349
Birnboim, Y., Dekel, A., & Neistein, E. 2007, MNRAS, 380, 339
Blitz, L., & Rosolowsky, E. 2006, ApJ, 650, 933
Blumenthal, G. R., Faber, S. M., Flores, R., & Primack, J. R. 1986, ApJ, 301, 27
Bouché, N. et al. 2007a, ApJ, 671, 303
Bouché, N., Murphy, M. T., Péroux, C., Davies, R., Eisenhauer, F., Förster Schreiber, N. M., & Tacconi, L. 2007b, ApJ, 669, L5
Bournaud, F., Elmegreen, B. G., & Elmegreen, D. M. 2007, ApJ, 670, 237
Brinchmann, J., Charlot, S., White, S. D. M., Tremonti, C., Kauffmann, G., Heckman, T., & Brinkmann, J. 2004, MNRAS, 351, 1151
Bruzual, G., & Charlot, S. 2003, MNRAS, 344, 1000
Burkert, A. et al. 2010, ApJ, submitted (arXiv:0907.4777)
Cantalupo, S. 2010, MNRAS, 403, L16
Catinella, B. et al. 2010, MNRAS, 403, 683
Cattaneo, A., Dekel, A., Devriendt, J., Guiderdoni, B., & Blaizot, J. 2006, MNRAS, 370, 1651
Cattaneo, A., Dekel, A., Faber, S. M., & Guiderdoni, B. 2008, MNRAS, 389, 567
Cattaneo, A., Mamon, G. A., Warnick, K., & Knebe, A. 2010, MNRAS, submitted (arXiv:1002.3257)
Chen, Y., Wild, V., Kauffmann, G., Blaizot, J., Davis, M., Noeske, K., Wang, J., & Willmer, C. 2009, MNRAS, 393, 406
Choi, J., & Nagamine, K. 2009, MNRAS, submitted (arXiv:0909.5425)
Cimatti, A., Daddi, E., & Renzini, A. 2006, A&A, 453, L29
Cowie, L. L., Songaila, A., Kim, T., & Hu, E. M. 1995, AJ, 109, 1522
Cresci, G. et al. 2009, ApJ, 697, 115
Daddi, E. et al. 2010a, ApJ, 713, 686
Daddi, E., Dannerbauer, H., Elbaz, D., Dickinson, M., Morrison, G., Stern, D., & Ravindranath, S. 2008, ApJ, 673, L21
Daddi, E. et al. 2009, ApJ, 694, 1517
—. 2007, ApJ, 670, 156
—. 2010b, ApJ, 714, L118
Dahlen, T., Mobasher, B., Dickinson, M., Ferguson, H. C., Giavalisco, M., Kretchmer, C., & Ravindranath, S. 2007, ApJ, 654, 172
Damen, M., Förster Schreiber, N. M., Franx, M., Labbé, I., Toft, S., van Dokkum, P. G., & Wuyts, S. 2009a, ApJ, 705, 617
Damen, M., Labbé, I., Franx, M., van Dokkum, P. G., Taylor, E. N., & Gawiser, E. J. 2009b, ApJ, 690, 937
Davé, R. 2008, MNRAS, 385, 147
Dekel, A., & Birnboim, Y. 2006, MNRAS, 368, 2
Dekel, A. et al. 2009a, Nature, 457, 451
Dekel, A., Sari, R., & Ceverino, D. 2009b, ApJ, 703, 785
Dekel, A., & Silk, J. 1986, ApJ, 303, 39
Dijkstra, M., Haiman, Z., Rees, M. J., & Weinberg, D. H. 2004, ApJ, 601, 666
Drory, N., & Alvarez, M. 2008, ApJ, 680, 41
Dutton, A. A., & van den Bosch, F. C. 2009, MNRAS, 396, 141
Dutton, A. A., van den Bosch, F. C., & Dekel, A. 2010, MNRAS, in press (arXiv/0912.2169)
Dutton, A. A., van den Bosch, F. C., Dekel, A., & Courteau, S. 2007, ApJ, 654, 27
Efstathiou, G., Davis, M., White, S. D. M., & Frenk, C. S. 1985, ApJS, 57, 241
Eke, V. R., Baugh, C. M., Cole, S., Frenk, C. S., King, H. M., & Peacock, J. A. 2005, MNRAS, 362, 1233
Elbaz, D. et al. 2007, A&A, 468, 33
Elmegreen, B. G., Bournaud, F., & Elmegreen, D. M. 2008, ApJ, 688, 67
Elmegreen, D. M., Elmegreen, B. G., Ravindranath, S., & Coe, D. A. 2007, ApJ, 658, 763
Epinat, B. et al. 2009, A&A, 504, 789
Erb, D. K. 2008, ApJ, 674, 151
Erb, D. K., Steidel, C. C., Shapley, A. E., Pettini, M., Reddy, N. A., & Adelberger, K. L. 2006a, ApJ, 647, 128
—. 2006b, ApJ, 646, 107
Förster Schreiber, N. M. et al. 2009, ApJ, 706, 1364
—. 2006, ApJ, 645, 1062
Gallazzi, A., Charlot, S., Brinchmann, J., White, S. D. M., & Tremonti, C. A. 2005, MNRAS, 362, 41
Genel, S., Bouché, N., Naab, T., Sternberg, A., & Genzel, R. . 2010, ApJ, in press (arXiv/1005.4058)
Genel, S. et al. 2008, ApJ, 688, 789
Genzel, R. et al. 2008, ApJ, 687, 59
—. 2006, Nature, 442, 786
—. 2010, MNRAS, in press (arXiv:1003.5180)
Giovanelli, R. et al. 2005, AJ, 130, 2613
Gnedin, N. Y. 2000, ApJ, 542, 535
González, V., Labbé, I., Bouwens, R. J., Illingworth, G., Franx, M., Kriek, M., & Brammer, G. B. 2010, ApJ, 713, 115
Grazian, A. et al. 2007, A&A, 465, 393
Guo, Q., White, S., Li, C., & Boylan-Kolchin, M. 2010, MNRAS, 404, 1111
Heavens, A., Panter, B., Jimenez, R., & Dunlop, J. 2004, Nature, 428, 625
Heckman, T. M., Lehnert, M. D., Strickland, D. K., & Armus, L. 2000, ApJS, 129, 493
Hernquist, L., & Springel, V. 2003, MNRAS, 341, 1253

Hopkins, A. M., & Beacom, J. F. 2006, ApJ, 651, 142
—. 2008, ApJ, 682, 1486
Iliev, I. T., Shapiro, P. R., & Raga, A. C. 2005, MNRAS, 361, 405
Immeli, A., Samland, M., Gerhard, O., & Westera, P. 2004, A&A, 413, 547
James, P. A., Prescott, M., & Baldry, I. K. 2008, A&A, 484, 703
Jimenez, R., Bernardi, M., Haiman, Z., Panter, B., & Heavens, A. F. 2007, ApJ, 669, 947
Kassin, S. A. et al. 2007, ApJ, 660, L35
Kennicutt, R. C. 1998, ARA&A, 36, 189
Kereš, D., Katz, N., Fardal, M., Dave, R., & Weinberg, D. H. 2009, MNRAS, 395, 160
Kereš, D., Katz, N., Weinberg, D. H., & Davé, R. 2005, MNRAS, 363, 2
Kravtsov, A. V. 2010, Advances in Astronomy, 2010
Krumholz, M. R., & Thompson, T. A. 2007, ApJ, 669, 289
Larson, R. B. 1974, MNRAS, 166, 585
Law, D. R., Steidel, C. C., Erb, D. K., Larkin, J. E., Pettini, M., Shapley, A. E., & Wright, S. A. 2007, ApJ, 669, 929
—. 2009, ApJ, 697, 2057
Lilly, S. J., Le Fevre, O., Hammer, F., & Crampton, D. 1996, ApJ, 460, L1
Lu, Y., & Mo, H. J. 2007, MNRAS, 377, 617
Madau, P., Ferguson, H. C., Dickinson, M. E., Giavalisco, M., Steidel, C. C., & Fruchter, A. 1996, MNRAS, 283, 1388
Martin, C. L. 2005, ApJ, 621, 227
Martin, C. L., & Kennicutt, Jr., R. C. 2001, ApJ, 555, 301
McBride, J., Fakhouri, O., & Ma, C. 2009, MNRAS, 398, 1858
McGaugh, S. S. 2005, ApJ, 632, 859
Meyer, M. J., Zwaan, M. A., Webster, R. L., Schneider, S., & Staveley-Smith, L. 2008, MNRAS, 391, 1712
Meyer, M. J. et al. 2004, MNRAS, 350, 1195
Mo, H. J., Mao, S., & White, S. D. M. 1998, MNRAS, 295, 319
Mo, H. J., Yang, X., van den Bosch, F. C., & Katz, N. 2005, MNRAS, 363, 1155
Mobasher, B. et al. 2009, ApJ, 690, 1074
Moster, B. P., Somerville, R. S., Maulbetsch, C., van den Bosch, F. C., Macciò, A. V., Naab, T., & Oser, L. 2010, ApJ, 710, 903
Murray, N., Quataert, E., & Thompson, T. A. 2010, ApJ, 709, 191
Nagamine, K., Ostriker, J. P., Fukugita, M., & Cen, R. 2006, ApJ, 653, 881
Navarro, J. F., & Steinmetz, M. 2000, ApJ, 538, 477
Neistein, E., & Dekel, A. 2008, MNRAS, 388, 1792
Neistein, E., van den Bosch, F. C., & Dekel, A. 2006, MNRAS, 372, 933
Neistein, E., & Weinmann, S. M. 2009, MNRAS, in press (arXiv:0911.3147)
Noeske, K. G. et al. 2007a, ApJ, 660, L47
—. 2007b, ApJ, 660, L43
Noguchi, M. 1998, Nature, 392, 253
Ocvirk, P., Pichon, C., & Teyssier, R. 2008, MNRAS, 390, 1326
Oesch, P. A. et al. 2010, ApJ, 709, L16
Oliver, S. et al. 2010, MNRAS, in press (arXiv/1003.24460)
Oppenheimer, B. D., & Davé, R. 2008, MNRAS, 387, 577
Pannella, M. et al. 2009, ApJ, 698, L116
Pawlik, A. H., & Schaye, J. 2009, MNRAS, 396, L46
Pieri, M. M., & Martel, H. 2007, ApJ, 662, L7
Puech, M. et al. 2008, A&A, 484, 173
Quinn, T., Katz, N., & Efstathiou, G. 1996, MNRAS, 278, L49
Rosenberg, J. L., & Schneider, S. E. 2003, ApJ, 585, 256
Rupke, D. S., Veilleux, S., & Sanders, D. B. 2005, ApJS, 160, 115
Santini, P. et al. 2009, A&A, 504, 751
Sawicki, M. et al. 2007, in Astronomical Society of the Pacific Conference Series, Vol. 380, Deepest Astronomical Surveys, ed. J. Afonso, H. C. Ferguson, B. Mobasher, & R. Norris, 433–+
Schaerer, D., & de Barros, S. 2009, A&A, 502, 423
—. 2010, A&A, 515, A73+
Schaye, J. et al. 2010, MNRAS, 402, 1536
Schiminovich, D. et al. 2005, ApJ, 619, L47
Schmidt, M. 1959, ApJ, 129, 243
—. 1963, ApJ, 137, 758
Shankar, F., Lapi, A., Salucci, P., De Zotti, G., & Danese, L. 2006, ApJ, 643, 14
Shapiro, K. L. et al. 2008, ApJ, 682, 231
—. 2009, ApJ, 701, 955
Shapley, A. E., Steidel, C. C., Pettini, M., & Adelberger, K. L. 2003, ApJ, 588, 65
Sheth, R. K., Mo, H. J., & Tormen, G. 2001, MNRAS, 323, 1
Somerville, R. S., Hopkins, P. F., Cox, T. J., Robertson, B. E., & Hernquist, L. 2008, MNRAS, 391, 481
Springel, V., Frenk, C. S., & White, S. D. M. 2006, Nature, 440, 1137
Springel, V., & Hernquist, L. 2003, MNRAS, 339, 312
Stark, D. P., Ellis, R. S., Bunker, A., Bundy, K., Targett, T., Benson, A., & Lacy, M. 2009, ApJ, 697, 1493
Stewart, K. R., Bullock, J. S., Wechsler, R. H., Maller, A. H., & Zentner, A. R. 2008, ApJ, 683, 597
Tacconi, L. J. et al. 2010, Nature, 463, 781
Thomas, D., Maraston, C., Bender, R., & Mendes de Oliveira, C. 2005, ApJ, 621, 673
Thomas, D., Maraston, C., Schawinski, K., Sarzi, M., & Silk, J. 2010, MNRAS, 404, 1775
Thoul, A. A., & Weinberg, D. H. 1996, ApJ, 465, 608
Tully, R. B., & Fisher, J. R. 1977, A&A, 54, 661
Tully, R. B., & Pierce, M. J. 2000, ApJ, 533, 744
van den Bergh, S. 1962, AJ, 67, 486
van den Bosch, F. C. 2002, MNRAS, 331, 98
van den Bosch, F. C., Abel, T., & Hernquist, L. 2003a, MNRAS, 346, 177
van den Bosch, F. C., Mo, H. J., & Yang, X. 2003b, MNRAS, 345, 923
van den Bosch, F. C. et al. 2007, MNRAS, 376, 841
van Starkenburg, L., van der Werf, P. P., Franx, M., Labbé, I., Rudnick, G., & Wuyts, S. 2008, A&A, 488, 99
Verma, A., Lehnert, M. D., Förster Schreiber, N. M., Bremer, M. N., & Douglas, L. 2007, MNRAS, 377, 1024
Wechsler, R. H., Bullock, J. S., Primack, J. R., Kravtsov, A. V., & Dekel, A. 2002, ApJ, 568, 52
White, S. D. M., & Frenk, C. S. 1991, ApJ, 379, 52
Wilkins, S. M., Trentham, N., & Hopkins, A. M. 2008, MNRAS, 385, 687
Wong, O. I. et al. 2006, MNRAS, 371, 1855
Wong, T., & Blitz, L. 2002, ApJ, 569, 157
Wright, S. A. et al. 2007, ApJ, 658, 78
Yabe, K., Ohta, K., Iwata, I., Sawicki, M., Tamura, N., Akiyama, M., & Aoki, K. 2009, ApJ, 693, 507
Zhang, W., Li, C., Kauffmann, G., Zou, H., Catinella, B., Shen, S., Guo, Q., & Chang, R. 2009, MNRAS, 397, 1243
Zwaan, M. A., & et al. 2003, AJ, 125, 2842

APPENDIX

SPECIFIC SFR IN THE EARLY UNIVERSE

Upon completion of this work, several groups have used deep *Hubble Space Telescope* data to their limit and published constraints on the SFR sequence beyond $z = 4$ (Stark et al. 2009), at $z = 5$ (Yabe et al. 2009), and $z = 7$ (González et al. 2010). As shown in Fig. 13, some groups (Stark et al. 2009; González et al. 2010) find that the SFR sequence does no longer evolve, i.e., the sSFR remains constant from $z \sim 4$ to $z \sim 7$, while Schaerer & de Barros (2010) find moderate and Yabe et al. (2009) strong evolution (see also Sawicki et al. 2007). The analysis of Schaerer & de Barros (2010) includes the sample of González et al. (2010) with the added WFC3 data from Oesch et al. (2010). Given that it is a challenge to derive accurate (dust-corrected) SFR and stellar masses at those redshifts in a self-consistent way, it may be premature to view the (non-)evolution of González et al. (2010) beyond $z = 2$ as definitely understood.

Assumptions in the model

Would the non-evolution of sSFR be real claimed by González et al. (2010), could the discrepant results of our model be due to some of our assumptions? Our model fails to indicate the turn over of González et al. (2010) in the evolution of sSFR(z) beyond $z = 2$ as shown in Figure 13. We turn to some of our assumptions in order to examine the robustness of this failed prediction. Could our model be modified in such a way to account for this apparent non-evolution of sSFR? Our main assumption, the accretion mass floor $M_{\rm min}$, only alters the mass index of the SFR sequence, but does not alter its redshift evolution. An assumption certain to break down at $z > 4$ is our assumed constant recycling fraction R. Indeed, R is a strong function of stellar ages (Bruzual & Charlot 2003) for ages < 1 Gyr. In order to understand how this affects our calculations in the first Gyr, we note that R affects the SF efficiency. The recycled fraction R is low at early times, meaning that the gas consumption is more efficient via the $(1-R)$SFR factor in Equation 3. Since the SF efficiency is increased, the steady state solution is reached faster, i.e., sSFR(z) is going to be set by the redshift dependence of the accretion rate sooner. Therefore, a more realistic $R(t)$ will not work in the right direction.

At those early times, the main assumption to break down in our model is related to the steady-state solution. As detailed in Section 3.1, galaxies in our model are out of the steady-state solution beyond $z > 5$. Therefore, the assumption made for the SF timescale (or efficiency), namely that $t_{\rm sfr}$ scales with the halo dynamical time $t_{\rm dyn}$ may break down: gas (or fuel for SF) is pouring at a rate faster than it can be consumed implying that the SF efficiency may be far from the local value. A more efficient gas consumption (shorter SF time scale) at early times means that the steady-state solution is reached more rapidly. This will only exacerbate the discrepancy between the z =4–8 data and the model. A less efficient gas consumption (longer SF time scale) at early times means that the SFR is increasing to some power of time t or redshift $(1 + z)$. Thus, the sSFR is always going to be proportional to sSFR(t) $\propto 1/t$.

Therefore, upon examining our assumptions, we find that the non-evolution of sSFR beyond $z = 2$ cannot be achieved easily. In other words, the evolution of sSFR beyond $z = 4$ is giving strong constraints on early galaxy formation. Taken at face-value, the González et al. (2010) results are going to be extremely challenging for any theoretical model.

Assumptions in the observations

In the observations, in order to fit the observed SEDs, one has to assume (i) a SFH, and (ii) treat the nebular emission lines consistently (Schaerer & de Barros 2009). These two can affect the sSFR significantly. For instance, at high SFRs and young ages, the nebular emission lines (e.g., [O III], $H\beta$) can affect the color significantly (Schaerer & de Barros 2009; Yabe et al. 2009, Finlator, in prep.). When this is omitted, the resulting Balmer break is overestimated, and hence the stellar mass, leading to an underestimated sSFR.

Similarly, the SFH can have a strong impact on the derived sSFR. At $z = 2$, the often assumed 'constant SFH' works generally well (e.g. Förster Schreiber et al. 2009) and this assumption is in good agreement with the growth predicted (see Fig. 6 and Section 3.1). At $z > 5$, different groups make different assumptions. For example, González et al. (2010) prefer a constant SFH, while Stark et al. (2009) and Schaerer & de Barros (2010) use an exponentially declining SFH with a range of ages. Unfortunately, the SFH is difficult to constrain from the data themselves, but has a significant impact on the sSFR. Indeed, if SFR(t) is constant, then sSFR goes as $1/t$. If SFR(t) is declining exponentially, then $M_\star(t)$ is dominated by the initial SFR at $t = t_0$ ($M_\star \simeq \exp(-t_0/\tau)$), and sSFR is dominated by the age $\Delta t = t - t_0$, with sSFR$\propto \exp(-\Delta t/\tau)$. If SFR($t$) is increasing exponentially, then $M_\star(t)$ is proportional to $\exp(+t/\tau)$, and the current SFR is also $\propto \exp(+t/\tau)$. Hence, the sSFR is constant in this case.

Given the short times between $z = 5$, $z = 6$, and $z = 7$, the various populations observed at these epochs are likely descendants and progenitors of one another and the inferred involution of sSFR(z) ought to be consistent with the assumed SFH. Currently, it appears that this self-consistency in the observational results is not present.

Star formation histories

At $z > 5$, galaxy formation is surely more uncertain. Proto-galaxies are more metal poor, the universe was just re-ionized, two facts that will impact molecular gas formation, hence the KS relation itself. Hence, several of our assumptions are likely to fail at those early epochs. However, a robust and generic feature of any model at those epochs is the rapid growth rate $\dot{M}$, which implies that the SFHs are very far from exponentially declining. In order to guide interested readers with SFHs appropriate in this regime of steady growth (at $z > 4$), we note that in the redshift

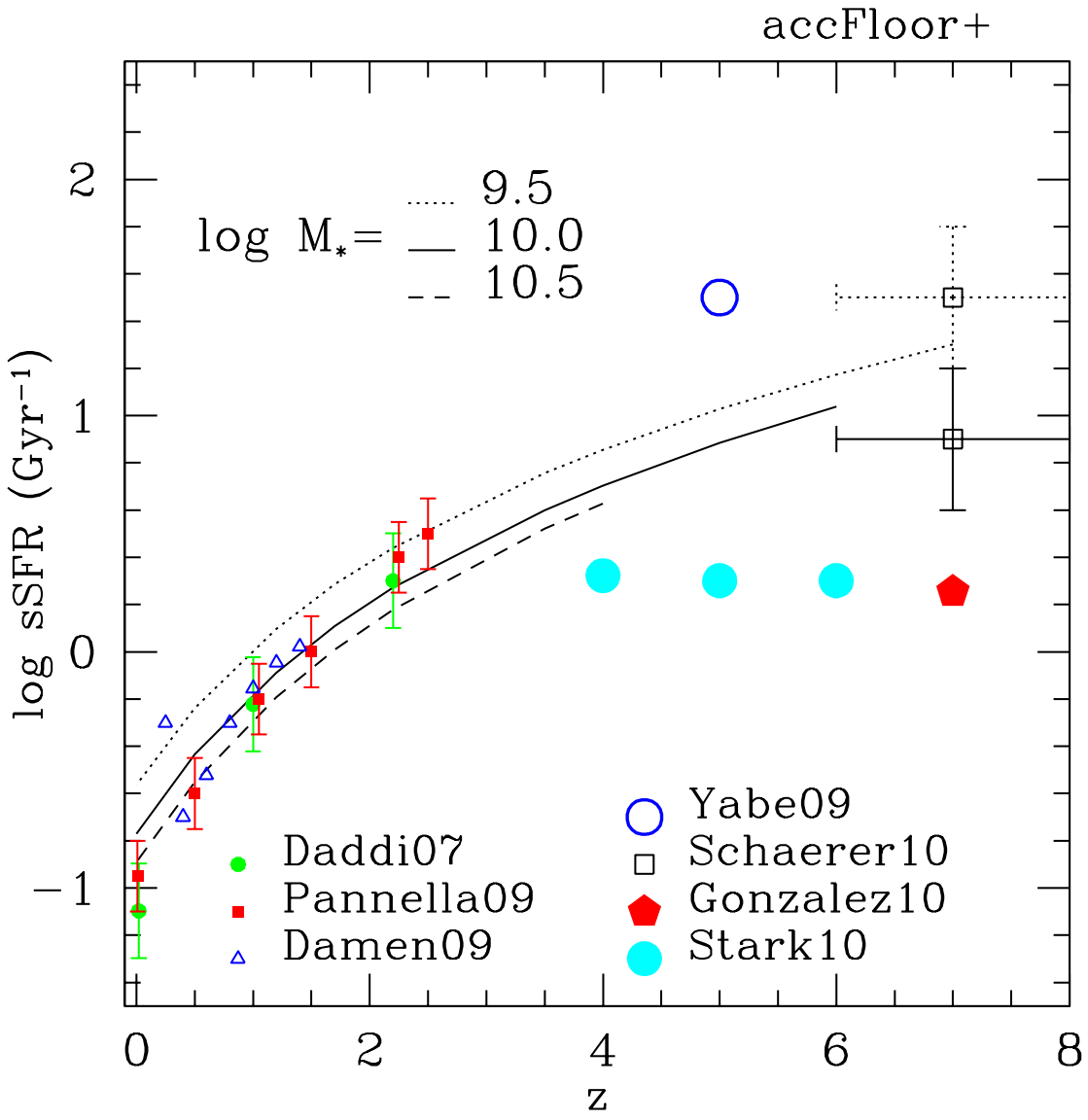

FIG. 13.— The evolution of sSFR at high-redshifts. The lines show the predicted predicted evolution by our model ('accFloor+') at a fixed $M_\star$ as in Fig. 6. At $z < 4$, the data points are as in Fig. 6. At $z > 4$, the González et al. (2010) and Stark et al. (2009) results indicate no-evolution of the sSFR, while Yabe et al. (2009) indicates strong evolution. This clear lack of agreement among the various groups reflects the challenges in deriving accurate (dust-corrected) SFR and stellar masses at those redshifts in a self-consistent way (see text). The re-analysis of the González et al. (2010) sample by Schaerer & de Barros (2010) using the recent WFC3 data is shown with the open square with solid error bars (with $\log M_\star \simeq 9.5$). The 'faint' sample of Schaerer & de Barros (2010) with $\log M_\star \simeq 8.0$ is shown with the square with dotted error bars.

range $z = 5$ to $z = 7$, our SFHs are approximate *increasing* exponential, SFR(t)$\propto \exp(+t/\tau)$, with a time scale τ close to ~ 0.5 Gyr as shown in Fig. 14 with the dotted line. Using $\tau = 0.5$ Gyr, one can approximate the SFR(t) with

$$\mathrm{SFR}(t) \propto e^{(+t/\tau)} \text{for times } t > t_f, \tag{A1}$$

where the formation time t_f is given by $(1 + z_f) \simeq 0.4 \times M_\star^{0.13}$. As Fig. 14 shows that τ varies from 0.3 Gyr to 0.6 Gyr between $z = 5$ and $z = 7$, a physically motivated form (dashed line) is

$$\mathrm{SFR}(t) = 100 e^{(+(t-t_c)/\tau(z))} \text{with } \tau(z) = 0.5\mathrm{Gyr}\left(\tfrac{1+z}{1+z_b}\right)^{-2.2}, \tag{A2}$$

where t_c and z_b are the fitted parameters. Table 2 lists the fitted parameters. A more accurate fit is obtained using polynomials of the type $a_0 + a_1 U^1 + a_2 U^2$, where $U = t/(10^9 \mathrm{yr})$, and shown as the red curves in Fig. 14.

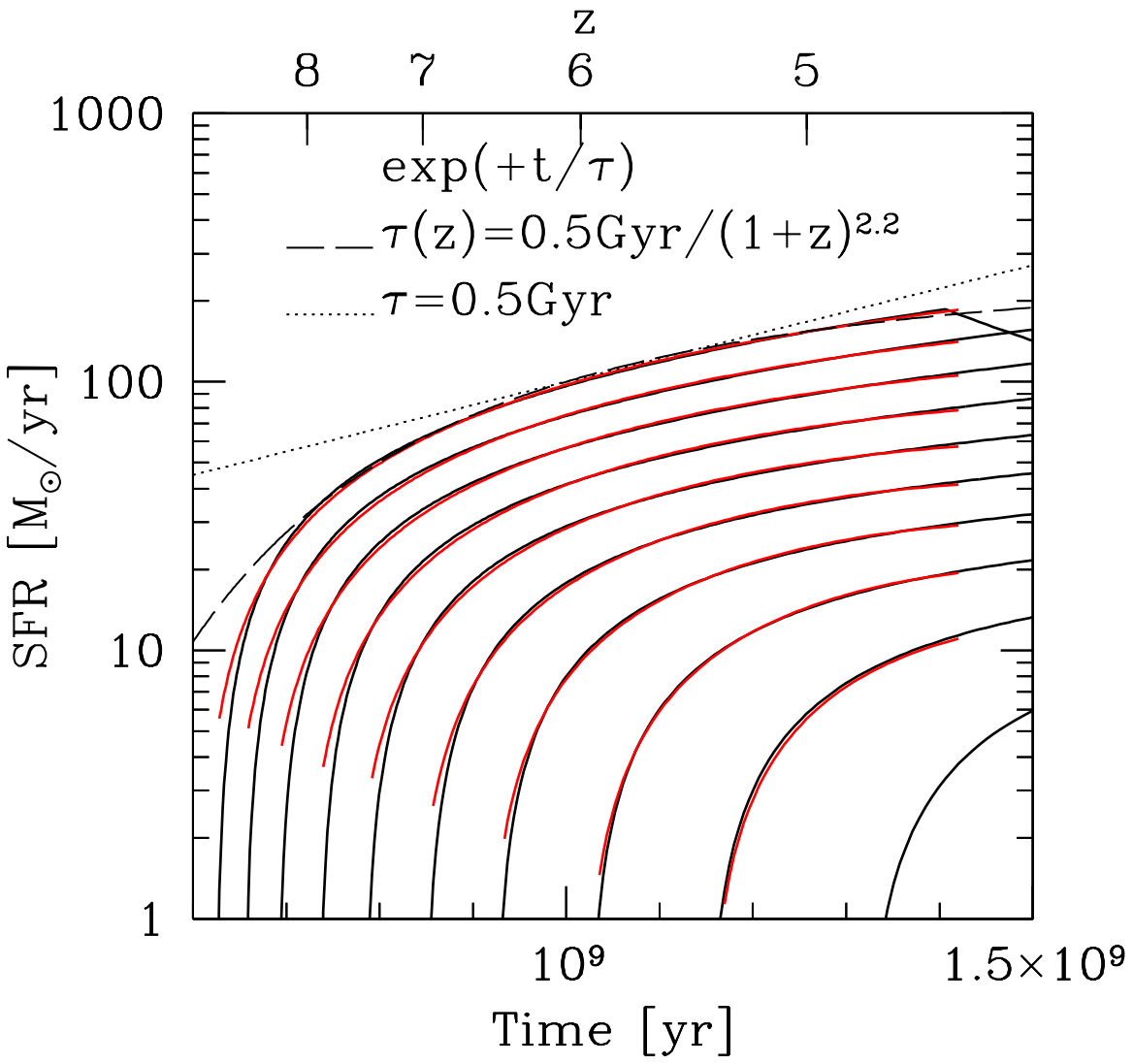

FIG. 14.— At $z > 4.5$, the star-formation histories are close to being *increasing* exponential, $\mathrm{SFR}(t) \propto e^{+t/\tau}$ with $\tau \sim 0.5$ Gyr (dotted line). Motivated by the halo growth, the dashed line shows an evolving tau $\tau(z) \simeq 0.5\mathrm{Gyr}\left(\frac{1+z}{1+5.5}\right)^{-2.2}$. The red curves shows second order polynomial fits.

Halo ID	t_c (Gyr)	z_b	$M_\star(z=4)$
8	1.73±0.03	1.63±0.10	6.9E+8
9	2.38±0.10	4.32±0.23	2.1E+8
10	3.01±0.19	6.69±0.39	4.3E+9
11	3.19±0.20	8.31±0.43	7.4E+9
12	2.67±0.10	8.37±0.30	1.1E+10
13	2.08±0.04	7.82±0.17	1.7E+10
14	1.63±0.01	7.04±0.09	2.4E+10
15	1.336±0.004	6.39±0.04	3.3E+10
16	1.141±0.001	5.84±0.03	4.3E+10
17	1.008±0.001	5.38±0.02	5.1E+10

TABLE 2
PARAMETERS FOR THE SFHS USING EQUATION A2 .